Emeis, K.-C., Robertson, A.H.F., Richter, C., et al., 1996
Proceedings of the Ocean Drilling Program, Initial Reports, Vol. 160

6. Site 965[1]

Shipboard Scientific Party[2]

HOLE 965A

Date occupied: 24 March 1995

Date departed: 27 March 1995

Time on hole: 2 days, 10 hr

Position: 33°55.080′N, 32°42.785′E

Bottom felt (drill-pipe measurement from rig floor, m): 1517.7

Distance between rig floor and sea level (m): 11.1

Water depth (drill-pipe measurement from sea level, m): 1506.6

Total depth (from rig floor, m): 1768.1

Penetration (m): 250.4

Number of cores (including cores having no recovery): 27

Total length of cored section (m): 250.4

Total core recovered (m): 42.8

Core recovery (%): 17.0

Oldest sediment cored:
Depth (mbsf): 250.40
Nature: limestone (brecciated bioclastic grainstone)

Principal results: Site 965 is one of four in a north-south transect designed to test the tectonic hypothesis that the Eratosthenes Seamount is a crustal fragment in the processes of breaking up and subsiding in the collision zone between the African and Eurasian plates. The site is located on the fault-controlled upper slope of the Eratosthenes Seamount. To be successful, drilling at this locality needed to establish the history of vertical tectonic motion of this part of the seamount and the age and paleoenvironments of the lithostratigraphic units, which were expected to include Pliocene-Quaternary deep-sea sediments and Miocene, or older, units. The principal objectives were achieved by drilling to 250 mbsf in Hole 965A.

The upper part of the succession comprises 23 m of Pliocene-Quaternary nannofossil muds and oozes, with rare sapropels. The succession shows much evidence of tectonic instability, as recorded by evidence of sediment mass movement, faulting, and depositional hiatuses. Beneath this is a distinctive thin unit (approximately 6 m) dominated by clays with scattered angular carbonate clasts. This unit contains aragonite and dolomite and locally abundant ostracode carapaces, and is interpreted to have accumulated in low- to elevated-salinity settings of early Pliocene or possibly Messinian age. Below the thin unit is a 200-m-thick interval in which mainly limestone was recovered. Interpretation of the borehole logs suggests that relatively thin-bedded units (i.e., limestones) are intercalated with more abundant fine-grained sediment that is probably micritic. The composition of the limestones indicates accumulation in a shallow-water, possibly lagoonal, setting adjacent to reef buildups. There is some evidence of high-angle faulting.

The sequence is interpreted to indicate accumulation on a subsiding carbonate platform, probably in the Miocene, followed by minor accumulation during the Messinian salinity crisis. Strong tectonic subsidence was evident by the early Pliocene, and accumulation in a tectonically unstable, deep-water setting persisted during the Pliocene-Quaternary.

BACKGROUND AND OBJECTIVES

Site 965 is the first in the transect of holes drilled across the Eratosthenes Seamount to the Cyprus margin (Figs. 1, 2). The site was selected on the upper northern slope of the Eratosthenes Seamount in an area where the interpretation of seismic records suggests that the Pliocene-Quaternary is relatively thin (approximately 50 m, compared to approximately 100 m on the crestal area of the seamount). The site was intended to test one part of the tectonic hypotheses that Eratosthenes Seamount is a fragment of continental crust that is in the process of collision with the Cyprus active margin, a segment of the Africa-Eurasia convergence zone in the Eastern Mediterranean (Robertson, 1990; Robertson et al., 1994a, 1995; Limonov et al., 1994). In this hypothesis, the present-day northern site of the seamount might reveal evidence of subsidence and breakup.

To test the hypothesis effectively for the transect as a whole, it was necessary to answer the following questions: (1) what is the paleoenvironmental setting and depth of deposition of the upper, nearly transparent seismic interval of inferred Pliocene-Quaternary age; (2) what are the timing and processes of subsidence of the seamount, if observed; and (3) what are the age, lithology, and origin of the prominent reflector beneath the inferred Pliocene-Quaternary succession?

In this context, the objectives at Site 965 specifically were (1) to date the upper relatively transparent interval; (2) to determine if this succession showed evidence of tectonic instability, notably mass-wasting processes and, if so, over what time interval; (3) to determine the nature of the prominent underlying reflector, possibly equivalent to the "M" reflector in the adjacent basins; (4) to determine the lithol-

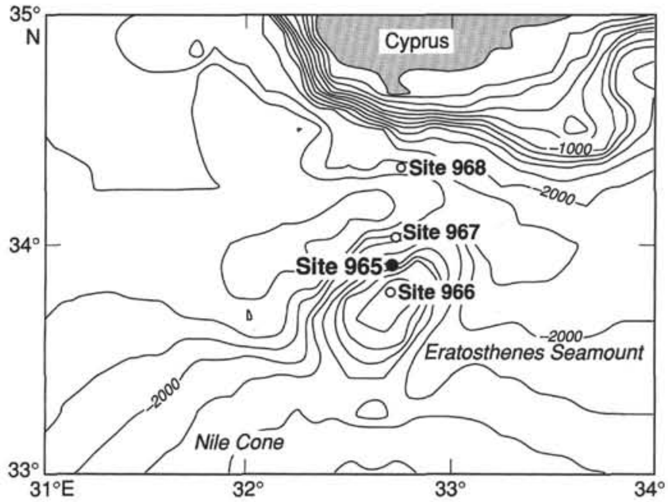

Figure 1. Outline of the bathymetry showing transect Site 965 in relation to the seafloor of the Eratosthenes Seamount and the Cyprus margin.

[1]Emeis, K.-C., Robertson, A.H.F., Richter, C., et al., 1996. *Proc. ODP, Init. Repts.,* 160: College Station, TX (Ocean Drilling Program).
[2]Shipboard Scientific Party is given in the list preceding the Table of Contents.

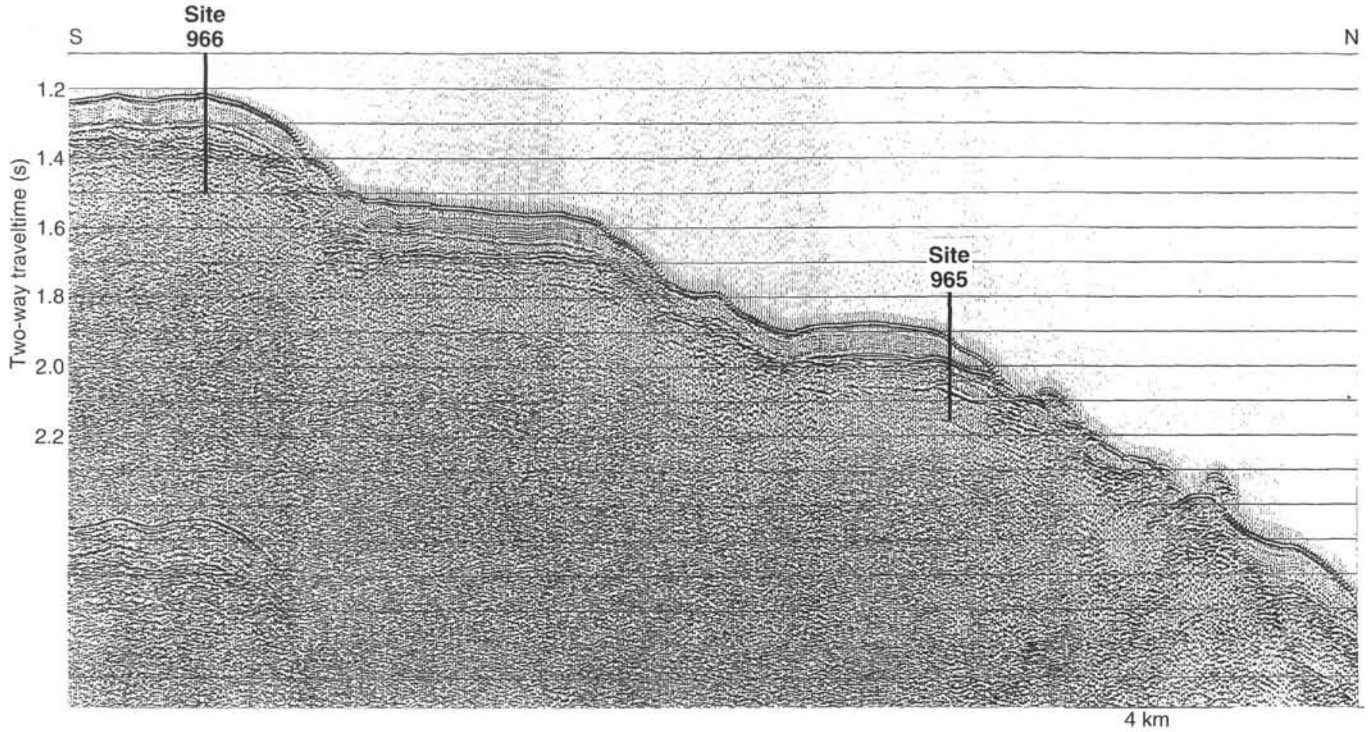

Figure 2. Northern part of the Eratosthenes plateau area and the northern slope of the seamount showing the location of Site 965. Note the normal faults downstepping to the north.

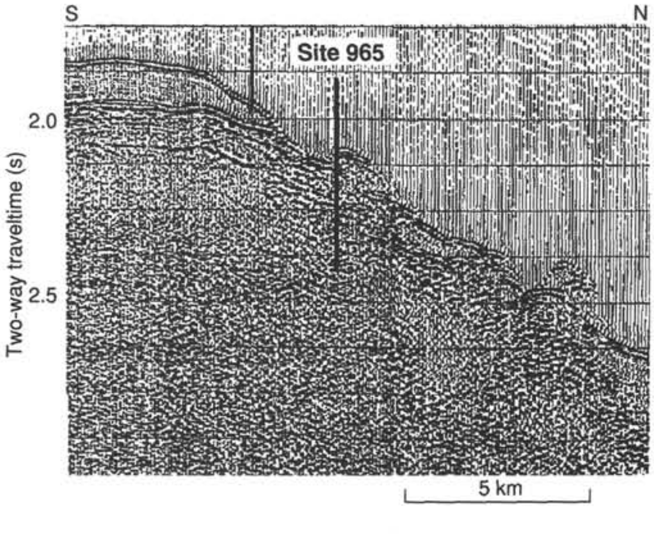

Figure 3. North-south single-channel seismic profile of the location of Site 965. Note that the location is in an area where the Pliocene-Quaternary is thin owing to downslope mass wasting. The crossing lines show that Site 965 is located near the crest of a small north-south-trending ridge surrounded by steep slopes interpreted as fault scarps. TREDMAR-3 Line 120, 1993.

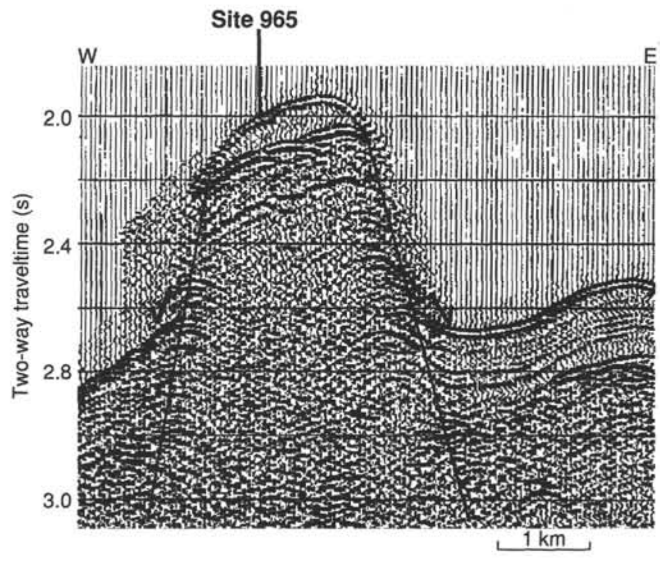

Figure 4. East-west single-channel seismic profile of the location of Site 965. Note the prominent north-south-trending ridge on which Site 965 is located.

ogy, age, and paleoenvironments of the underlying reflective seismic unit; and (5) to infer the subsidence history of the site in relation to the collision hypothesis for Eratosthenes Seamount.

GEOLOGICAL SETTING

Site 965 is located on the upper northern slopes of the Eratosthenes Seamount (Fig. 3). As outlined in the "Principal Results" section to this chapter, the seamount is inferred to be in the process of collision along the Cyprus active margin (Robertson et al., 1994b), but the timing of any such collision was until now unknown. In the area of Site 965, where much of the inferred Pliocene-Quaternary succession is absent, the prominent reflector underlying the inferred Pliocene-Quaternary appears on *Gelendzhik* Line 120 to lie close to the seafloor and to be strongly disrupted (Fig. 4).

Analysis of the TREDMAR-3 site-survey data and our underway seismic information (see "Site Geophysics" section, this chapter) confirm that Site 965 is located on the crest of a small northward-sloping ridge, bounded on both sides by steep slopes interpreted as fault scarps (Fig. 5). Traced northward across its plateau area, Eratosthenes Seamount is offset by a series of steps, both northward and

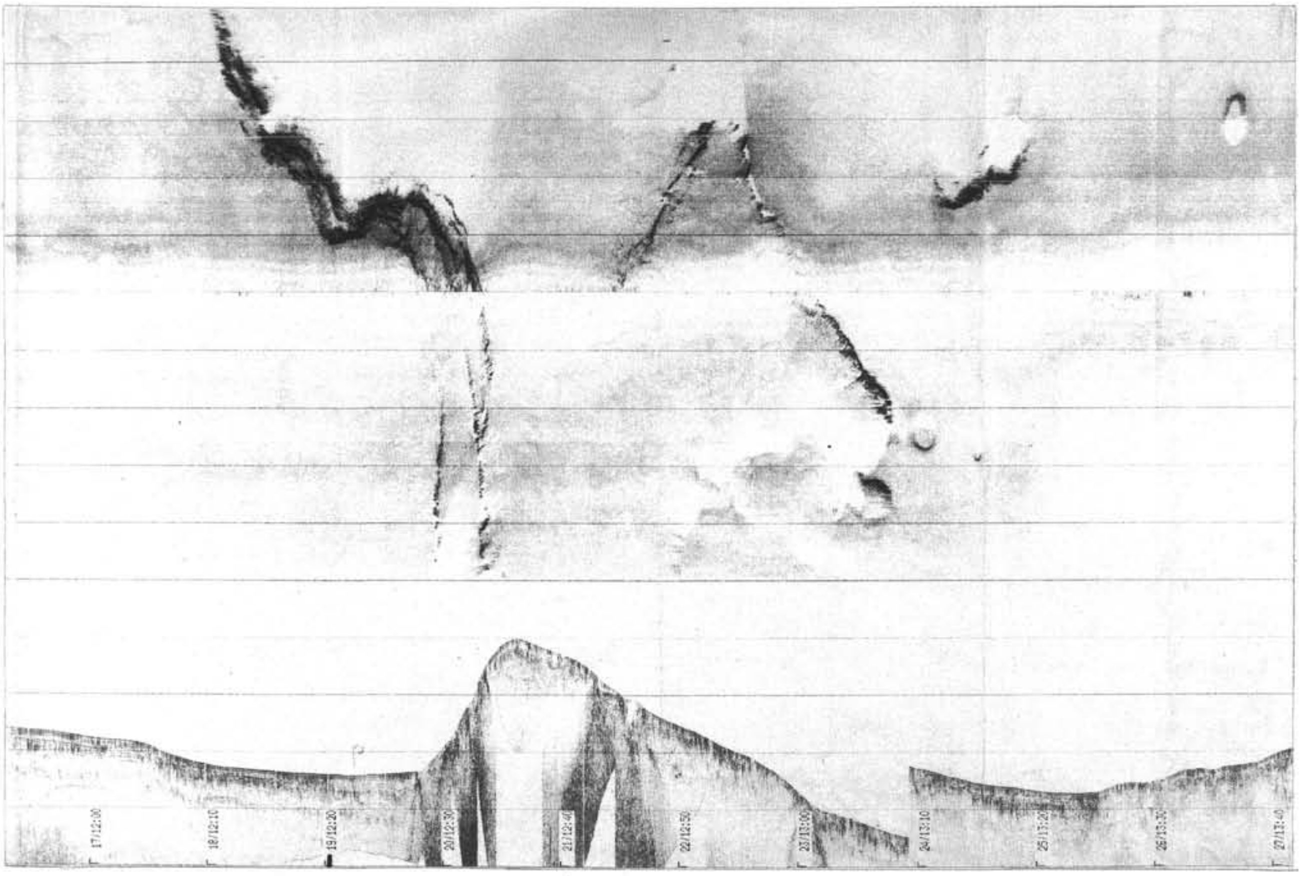

Site 965

Figure 5. Northwest-southeast MAK-1 narrow-beam side-scan image (Line 21, 1993) of the vicinity of Site 965. Note the highly irregular fault-controlled topography. Site 965 is on the crest of a small ridge.

southward, that are interpreted as normal faults, with offsets of approximately 200–220 m (Limonov and Woodside, 1994). A nearly transparent, inferred Pliocene-Quaternary succession is draped over these faults, suggesting that they essentially predate the underlying prominent reflector, which is offset. On the other hand, the Pliocene-Quaternary succession above the fault traces is itself offset and steepened, suggesting that some of the normal faults were active during the Pliocene-Quaternary. Observations using wide-beam (OKEAN) and narrow-beam (MAK-1) side-scan sonar suggest that some of the faults that lack sediment cover are recently active features (Alibes et al., 1994; Beijdorff et al., 1994).

The nearly flat, but somewhat downfaulted, plateau area of Eratosthenes Seamount culminates in a small slightly raised area, chosen as the location of Site 966. To the north, there is a gentle slope down to a first terrace. The break in slope is interpreted as an important steep normal fault. The nearly transparent inferred Pliocene-Quaternary succession remains undisrupted on the first terrace. Farther northward is a second slope interval, also controlled by inferred normal faulting down to a second terrace level, again with an intact inferred Pliocene-Quaternary succession. This is followed by a third slope interval, approximately 7 km long, of which the upper 1 km lacks any visible Pliocene-Quaternary sediment, whereas in the lower interval Pliocene-Quaternary sediment is again visible, but is disrupted by faults and slumps. Northward, the inferred Pliocene-Quaternary remains intact, but the slope remains relatively steep, broken by a small northward-inclined terrace.

Deep-tow data additionally show that the faults in the vicinity of Site 965 trend southwest-northeast. On the MAK-1 side-scan data, the faults are revealed as a highly reflective sonograph facies, with intervals up to 500 m wide at its base that are interpreted as mass-wasted material. Small reentrants into the fault scarps are interpreted as slump scars, or gullies (Beijdorff et al., 1994).

During the TREDMAR-3 cruise, a single gravity core was taken at the location of Site 965 and retrieved only 104 cm of nannofossil mud, including a 4-cm-thick carbonate-cemented unit containing foraminifers and traces of burrowing (Lucchi et al., 1994). This carbonate possibly originated as a hardground in an area of low or absent net sediment accumulation.

A sample of chalk dredged from the southern flank of the Eratosthenes Seamount during the 1987 cruise of *Academician Nikolai Strakhov* was initially thought to be of mid-Cretaceous age, based on lithologic correlation with carbonates in Syria. This sample was recently reexamined by Y. Mart, who confirmed the existence of open-marine chalk of early to mid-Miocene age. This was covered by a shallow-water limestone with black manganese-rich encrustations on three sides and contained neritic fossils of late Miocene age (Y. Mart, pers. comm., 1995). Interpretation of the seismic data suggests that the southern margin of Eratosthenes Seamount represents essentially the passive margin of an original structure, now shown by drilling at Site 965 to be a shallow-water carbonate buildup. The presence of an open-marine fauna from the southern Eratosthenes flank is in keeping with this interpretation.

OPERATIONS

Transit to Site 965 and Site Survey

The 749-nmi sea voyage to the proposed ESM sites required 59.9 hr at an average speed of 12.6 kt. Shipboard clocks were advanced 1 hr (0000–0100 hr) on 23 March to match European (Italian) daylight savings time. A 115-nmi seismic survey was run from south-to-north over proposed Sites ESM-1A, -2A, -3A, and -4A in 16.4 hr at 7.0 kt. *JOIDES Resolution* returned to Site ESM-2A, and a Datasonics 354M beacon (S/N 1240, 14.5 kHz) was deployed at 1828 hr on 24 March.

Site 965

Proposed Site ESM-2A was the first site drilled on the Eratosthenes Seamount as required by safety considerations. The same APC/XCB BHA used at Sites 963 and 964 was used at ESM-2A: a 10 ⅛-in. RBI PDC bit and APC/XCB BHA with a nonmagnetic drill collar.

The precision depth recorder indicated a seafloor depth of 1505.4 m below rig floor (mbrf). The first APC core from 1501.0 mbrf was a water core. The bit was lowered 8 m, and Hole 965A was spudded at 0035 hr on 25 March. A 0.76-m core was recovered, indicating a seafloor depth of 1506.6 mbrf by drill-pipe measurement. APC Cores 160-965A-1H through 4H were taken from 0 to 29.3 mbsf (Table 1), with 29.3 m cored and 29.87 m recovered (101.9% recovery). Core 160-965A-4H was oriented and had a partial stroke that bottomed in a hard clay and limestone. The maximum gas detected was 6 ppm methane.

XCB Cores 160-965A-5X through 27X were taken from 29.3 to 250.4 mbsf, with 221.1 m cored and 12.92 m recovered (5.8% recovery). XCB recovery was poor in the limestones and carbonate breccia. Erratic torque indicated extensive fracturing and 25-bbl high-viscosity gel mud sweeps were pumped with each core. The last two cores jammed in the shoe.

Logging Operations at Hole 965A

The hole was conditioned for logging with a short trip. No drag and only 1 m of fill indicated good hole conditions for logging. The hole was displaced with 120 bbl of 9.0-ppg sepiolite/seawater mud. The bit was positioned at 89.2 mbsf to log. Sonic, density neutron, and FMS logs were run to 1768.2 mbrf total depth with no fill. Logging finished at 0100 hr on 27 March, and the bit was pulled, clearing the rotary table at 0425 hr. The beacon was recovered, and the transit to Site 966 began at 0430 hr.

Table 1. Coring summary for Site 965.

Core	Date (March 1995)	Time (UTC)	Depth (mbsf)	Length cored (m)	Length recovered (m)	Recovery (%)
160-965A-						
1H	24	2250	0.0–0.8	0.8	0.76	95.0
2H	24	2330	0.8–10.3	9.5	9.98	105.0
3H	24	2355	10.3–19.8	9.5	9.97	105.0
4H	25	0035	19.8–29.3	9.5	9.16	96.4
5X	25	0230	29.3–38.8	9.5	0.32	3.4
6X	25	0310	38.8–48.3	9.5	0.31	3.3
7X	25	0355	48.3–57.9	9.6	0.10	1.0
8X	25	0540	57.9–67.5	9.6	0.26	2.7
9X	25	0650	67.5–77.1	9.6	0.90	9.4
10X	25	0800	77.1–86.8	9.7	0.21	2.2
11X	25	0905	86.8–96.4	9.6	0.27	2.8
12X	25	1010	96.4–106.0	9.6	0.70	7.3
13X	25	1125	106.0–115.7	9.7	0.55	5.7
14X	25	1300	115.7–125.4	9.7	0.83	8.6
15X	25	1415	125.4–135.1	9.7	0.82	8.5
16X	25	1525	135.1–144.7	9.6	0.93	9.7
17X	25	1640	144.7–154.3	9.6	0.76	7.9
18X	25	1810	154.3–163.9	9.6	0.10	1.0
19X	25	1920	163.9–173.6	9.7	0.45	4.6
20X	25	2035	173.6–183.1	9.5	0.39	4.1
21X	25	2150	183.1–192.6	9.5	0.36	3.8
22X	25	2300	192.6–202.2	9.6	0.09	0.9
23X	25	0015	202.2–211.9	9.7	0.47	4.8
24X	25	0130	211.9–221.5	9.6	0.85	8.9
25X	25	0310	221.5–231.1	9.6	0.82	8.5
26X	25	0520	231.1–240.8	9.7	1.41	14.5
27X	25	0715	240.8–250.4	9.6	1.02	10.6
Coring totals:				250.4	42.8	17.1

SITE GEOPHYSICS

This site was chosen on the basis of the thin to absent sedimentary layer over a strong reflector inferred to represent the Miocene/Pliocene transition. It is located near the northern edge of a small plateau on the upper part of the northern slope of Eratosthenes Seamount. The first survey line across it, in a south to north direction (Fig. 6) is almost identical to the original site survey line obtained in 1993 by *Gelendzhik*. The upper sedimentary layer, with a thickness of up to 150 ms two-way traveltime (TWT) (or approximately 125 m) on the upper plateau of Eratosthenes Seamount, thins northward in two stages, from about 100 to about 60 ms TWT thick across the step where Site 965 was to be drilled, eventually pinching out within the resolution of the seismic reflection profile (Fig. 7). On the slope to the north, slightly below the site, a large humped block of sediment lies over the strong reflector, which suggests that the sediments were thinned as the result of a large slide of the upper sedimentary unit.

The strong continuous reflector has a slightly greater amplitude at Site 965 than farther south in the shallower part of the seamount, which suggests a different facies of underlying rock. Movement of slide blocks and slumping above this horizon on the north slope of Eratosthenes Seamount, together with the character of the reflections, suggest that the underlying units are hard rock or more consolidated sediments. The survey data show deeper concave-upward reflectors beneath the strong reflector that further suggest that the strong reflector marks an unconformity (Fig. 7). If the angular discordance marks a period of shallow-water or subaerial erosion, then the strong reflector could be considered to represent the erosion surface with reefal units perhaps followed by deeper water sedimentary (pelagic or hemipelagic) deposition. On this basis, the reflector was inferred previously to mark the end of the Messinian desiccation and the return of marine deposition (e.g., Limonov et al., 1994).

The west to east crossing of the site showed it to be located on the top but near the edge of a roughly 2-km-wide ridge (see Fig. 4, "Geological Setting" section, this chapter). Because of the difference in the

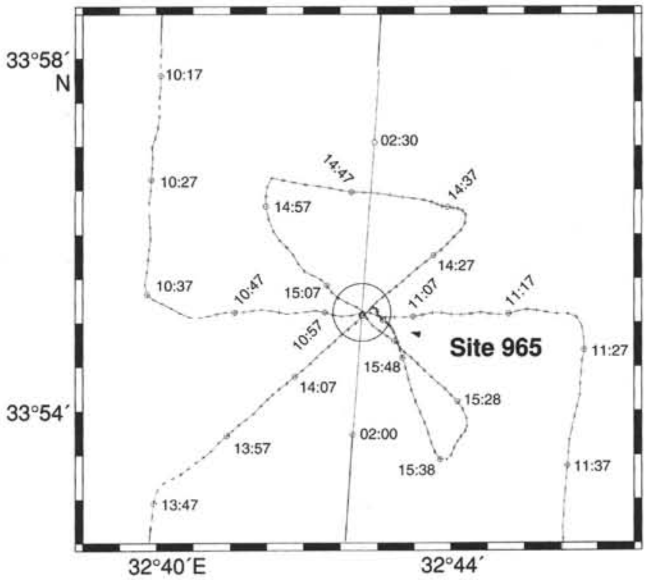

Figure 6. Location map showing the site-survey tracks across Site 965.

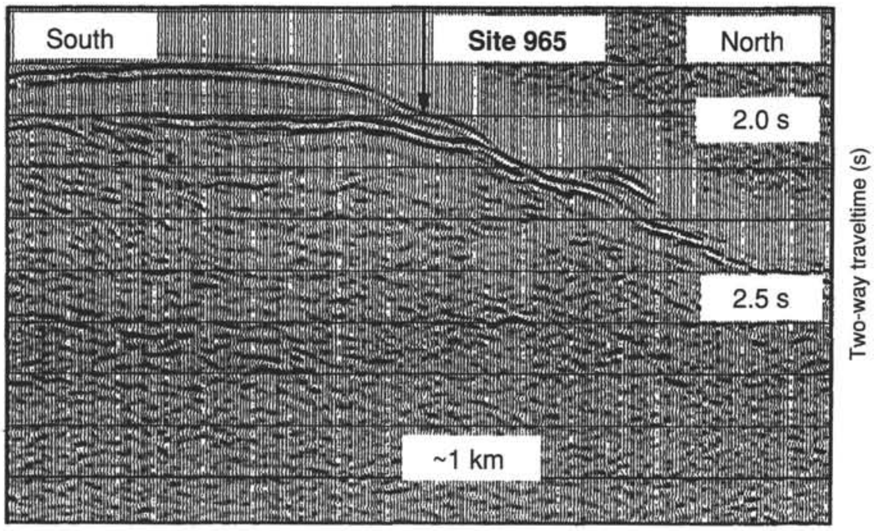

Figure 7. South to north seismic profile across Site 965 showing the thinned upper sedimentary unit above a strong continuous reflector.

appearance of the site on the two cross lines, two more survey lines were made across the site in different directions, creating, in the end, eight lines radiating from the site at 45° intervals. The additional survey lines showed that the site is located on a large promontory created probably by the removal of adjacent parts of the step by downslope mass wasting (Fig. 8; see also side-scan sonar data from farther along the promontory, in Fig. 5 of "Geological Setting" section, this chapter).

LITHOSTRATIGRAPHY

Hole 965A penetrated 250.4 m of calcareous ooze and clays overlying limestones. The unconsolidated material is principally nannofossil clay with limited intervals of foraminifer-bearing nannofossil clay and nannofossil ooze. Intercalated within the calcareous muds are several decimeter-thick, dark-colored sapropels that contain disseminated organic matter and pyrite in addition to the common components of the muds.

The calcareous muds overlie a 5.9-m-thick clay layer that rests unconformably on limestones. In general, the latter are biomicrites and biosparites that have undergone some recrystallization. Calcareous algae, foraminifers, and/or ooids are common and commonly dominate the clast composition; coral, mollusks, echinoderms, and other biota are subordinate, or absent.

Criteria employed in the lithostratigraphic description and classification at Site 965 included (1) visual observation of color; (2) visual observation of sedimentary structures, including bioturbation; (3) smear-slide and thin-section examination; (4) reflectance spectrophotometry measurements; (5) carbonate determinations; and (6) X-ray diffraction (XRD) analysis.

Description of Lithostratigraphic Units

The sediments recovered from Hole 965A can be divided into three lithostratigraphic units.

Lithostratigraphic Unit I

Description: Nannofossil ooze, clayey nannofossil ooze, nannofossil clay, and foraminifer sand
Interval: Sections 160-965A-1H-1 through 4H-2
Depth: 0–23.0 mbsf
Age: early Pleistocene to early Pliocene

Dominant Lithology

The dominant lithology of this unit is nannofossil ooze, clayey nannofossil ooze, nannofossil clay (all sporadically foraminifer bearing), and foraminifer sand. All are characterized by random alternations of color bands through a range of browns (10YR), grays (10Y), and greenish grays (5GY).

Smear-slide analyses reveal that the sediment is composed of between 30% and 80% nannofossils and between 5% and 60% clay. The clay content is unrelated to depth. Minor components include quartz, volcanic glass, inorganic calcite, and authigenic minerals (mainly pyrite).

XRD analyses of the dominant lithology show predominantly low-magnesium calcite with some quartz and minor amounts of high-magnesium calcite. Scattered small amounts of dolomite and halite (possibly from the seawater involved with drilling) are present. XRD of "whole-rock" specimens is not suited for the identification of clay minerals. However, weak signals in all analyses indicate that kaolinite appears ubiquitous. Small intervals of the section consist of gray (10Y 4/1) foraminifer sand and many of the light-colored intervals grade normally, on a decimeter to meter scale, from a foraminifer-dominated interval at the base to an ooze-dominated top.

Most of the sediments in this unit have undergone some degree of bioturbation, which increases markedly in the vicinity of some organic-rich minor lithologic intervals discussed below. Some of the light-colored intervals in this unit contain dark gray, iron(?)-sulfide-rich layers that are generally associated with bioturbation.

Toward the bottom of the unit (from about 16 mbsf; Section 160-965A-3H-1, 20 cm), the generally undisturbed nature of the sediments is disrupted markedly by a number of small faults and intraformational slumps, together with several small debris flows. Within the latter, clasts of both the dominant and minor lithologies are chaotically distributed.

Minor Lithologies

Sapropels

Intercalated within the dominant lithology are five discrete centimeter- to decimeter-thick dark olive gray (5Y 3/2) and very dark gray (5Y 3/1) intervals of nannofossil clay and clay (Fig. 9). All of these dark-colored intervals are enriched in pyrite and variable amounts of amorphous organic matter; some contain admixtures of volcanic glass, quartz, and possibly fragments of higher plant material.

Ash

Numerous thin (1–2 cm) ash layers occur throughout the section. They contain considerable (up to 80%) amounts of volcanic glass and commonly have foraminifers as a subdominant component. The fine-grained calcareous sediments usually contain a glass component

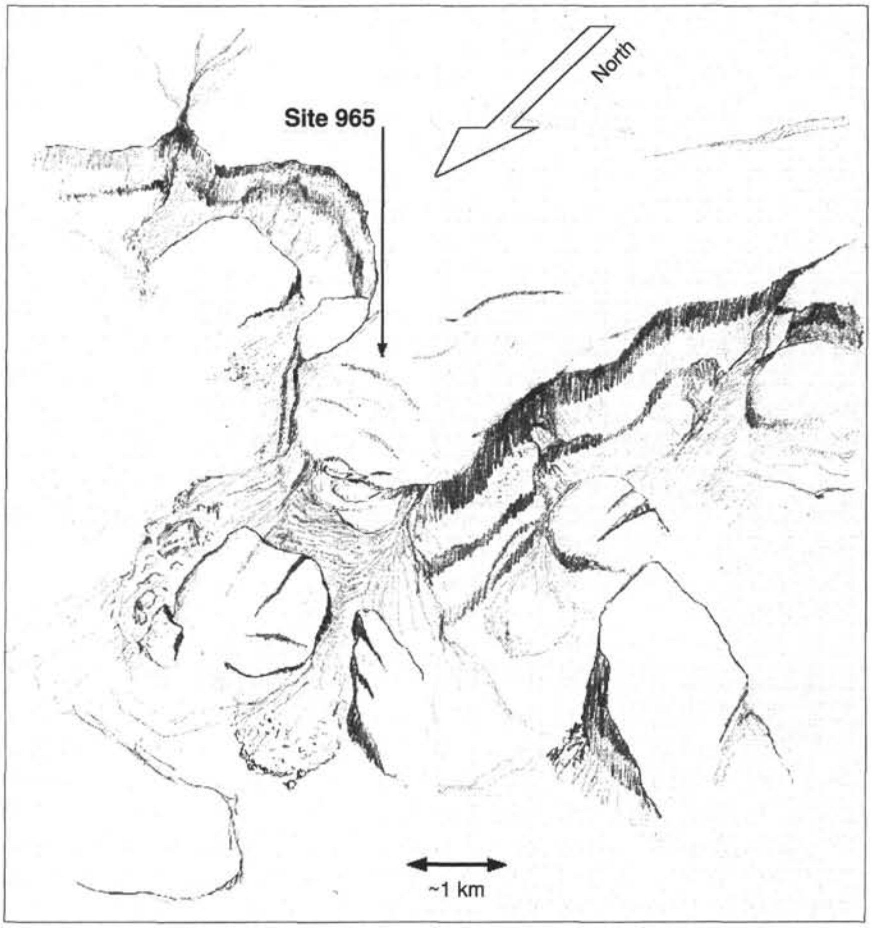

Figure 8. Interpretative sketch of the vicinity of Site 965 based on the four seismic cross lines.

probably derived from redistribution of the ash layers during bioturbation.

Lithostratigraphic Unit II

Description: Mottled calcareous clay with scattered carbonate clasts
Interval: Sections 160-965A-4H-3 through 4H-6
Depth: 23.0–29.3 mbsf
Age: early Pliocene

Directly underlying Unit I is a 6.3-m-thick section of mottled clays that contain clasts of chalky calcite up to 1 cm in diameter (below Section 160-965A-4H-3, 20 cm). Although these materials appear to have undergone some drilling disturbance, they have little resemblance to the overlying calcareous sediments. This part of the section is designated as Unit II in the lithostratigraphic succession.

At the top of the unit is a darker interval immediately underlain by a 20-cm-thick bed of unconsolidated calcareous nodules (Fig. 10). This material probably represents a paleosol with a calcrete-indurated B horizon. Smear slides of clays from below this interval are rich in aragonite and dolomite, both of which occur as small, well-developed crystals. In addition, numerous ostracode carapaces occur in some intervals within the unit (e.g., Section 160-965A-4H-4, 20 cm).

Lithostratigraphic Unit III

Description: Shallow-water carbonates
Interval: Cores 160-965A-5X through 27X
Depth: 29.3–250.4 mbsf
Age: Miocene(?)

Underlying the clay of Unit II is a continuous sequence of limestones that occupies the section to total depth of the hole at 250.4 mbsf. Core recovery from this interval was poor (generally <10%) and subtle details of the sequence remain unknown. Nevertheless, it was possible to identify the major lithotypes recovered and to reconstruct the depositional history of the unit.

The limestones vary from oosparites at the top through a range of biosparites and biomicrites to the bottom of the unit, where they are cut by numerous fractures filled with secondary calcite (Fig. 11) (see "Structural Geology" section, this chapter).

All limestones are recrystallized. However, neomorphism has not proceeded so far as to preclude identification of the major components and depositional textures in the rocks. Sparry calcite cement and/or neomorphed micrite are ubiquitous; almost all grains are bioclasts and only sporadic intraclasts occur in a few instances. The texture of the rocks changes to a large extent with composition. At the top of the unit the materials are oosparitic grainstones and packstones (Fig. 12), and deeper down (Core 160-965A-24X) encrusting calcareous algae dominate, and biomicritic wackestones and sporadic packstones occur (see Table 2, Fig. 13).

Depositional History

The depositional history of the succession recovered at Site 965 includes evidence of both shallow- and deep-water accumulation processes.

It is not clear if the entire succession in the unconsolidated sediments overlying the limestones is present in the section. Furthermore, the age of the limestones is inferred and nothing is known of what un-

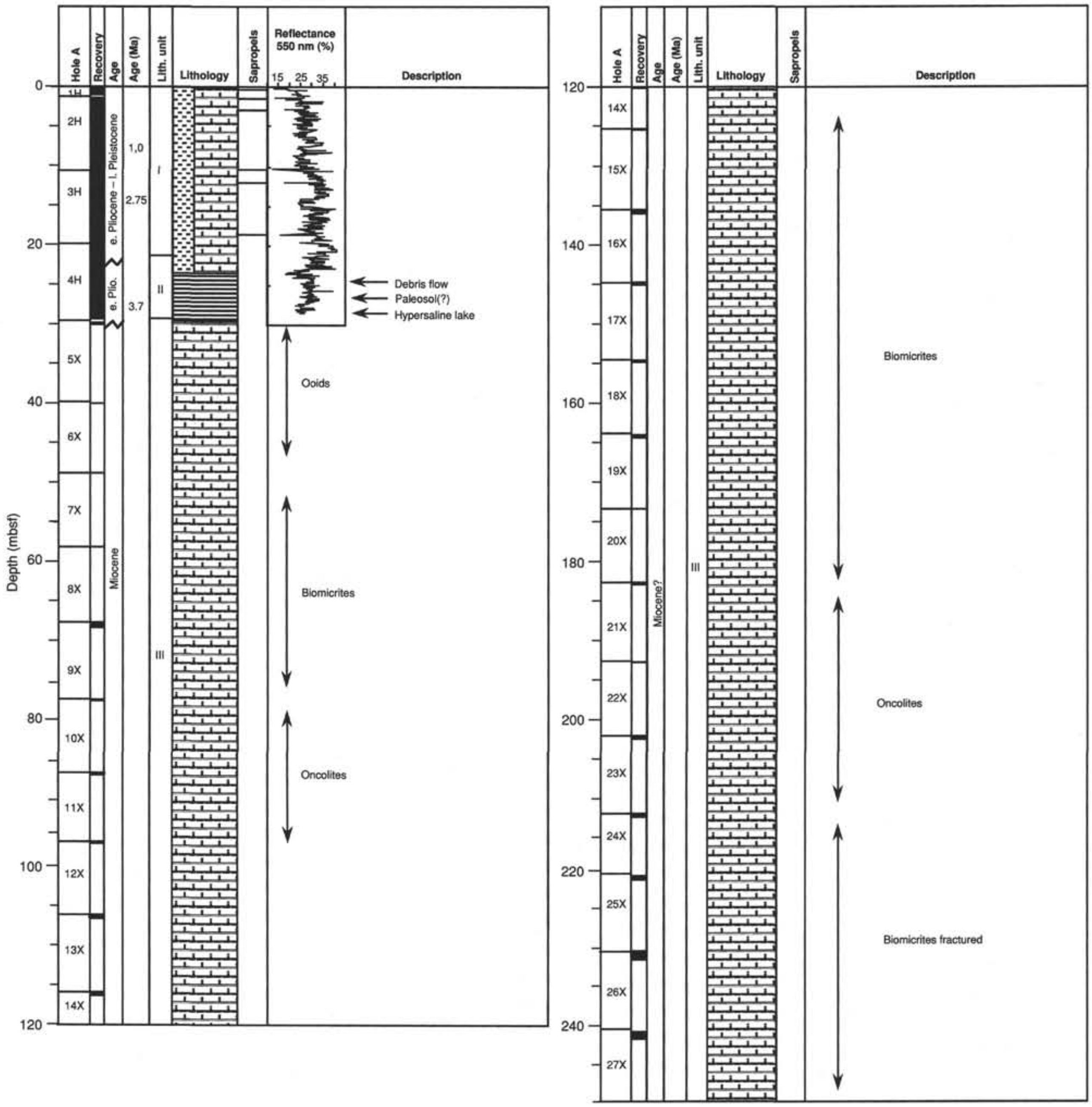

Figure 9. Core recovery, lithostratigraphic summary, color reflectance, and age information for Site 965.

derlies them (cf., Fig. 16, "Biostratigraphy and Sedimentation Rates" section, this chapter).

It is inferred that lithostratigraphic Unit III is the equivalent in age to Miocene rocks of similar character that occur on Cyprus (Robertson et al., 1991). Paleontological evidence suggests that Unit II is early Pliocene (3.75 Ma) in age and that Unit I ranges from the early Pliocene (<3.7 Ma) to the Holocene in age, with two significant hiatuses.

Using the recovered materials together with the time constraints, the following sequence of events may be reconstructed (Fig. 14).

Some time probably during the Miocene(?), on the area that now constitutes Eratosthenes Seamount, a marine setting conducive to shallow-water carbonate deposition, including coral reefs, developed. As these biotic communities continued to grow in shallow water, some degree of relative sea-level rise can be inferred, probably dominated by tectonic subsidence. Eustatic fluctuations may have occurred, but these are masked by the overall effects of the inferred tectonic subsidence.

The character of the environments in which the platform carbonates accumulated changed with time. These ranged from algal-dominated muddy lagoons possibly similar to the modern Florida Bay, through times when other biota dominated, depending on the ambient environmental conditions. Occasionally, these favored ooid formation and shoals and banks of these materials were distributed over the platform. Eventually, conditions favoring carbonate deposition ceased and the materials underwent lithification and subsequently minor recrystallization, mainly by meteoric-induced diagenesis as probably the dominant mechanism.

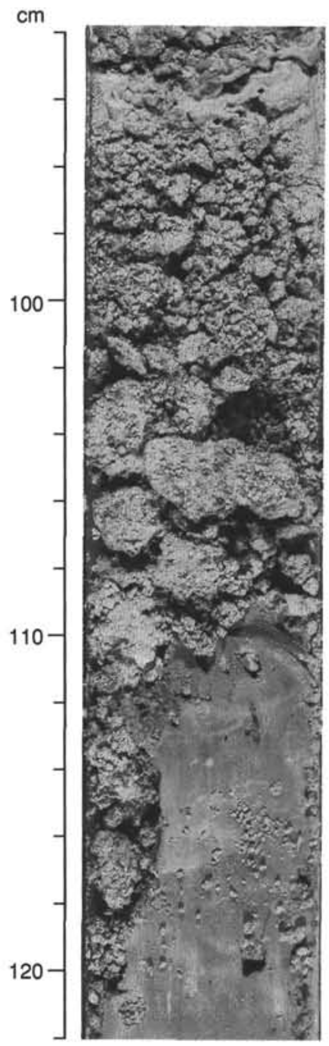

Figure 10. Caliche(?) layer below paleosol (Section 160-965A-4H-3, 92–122 cm).

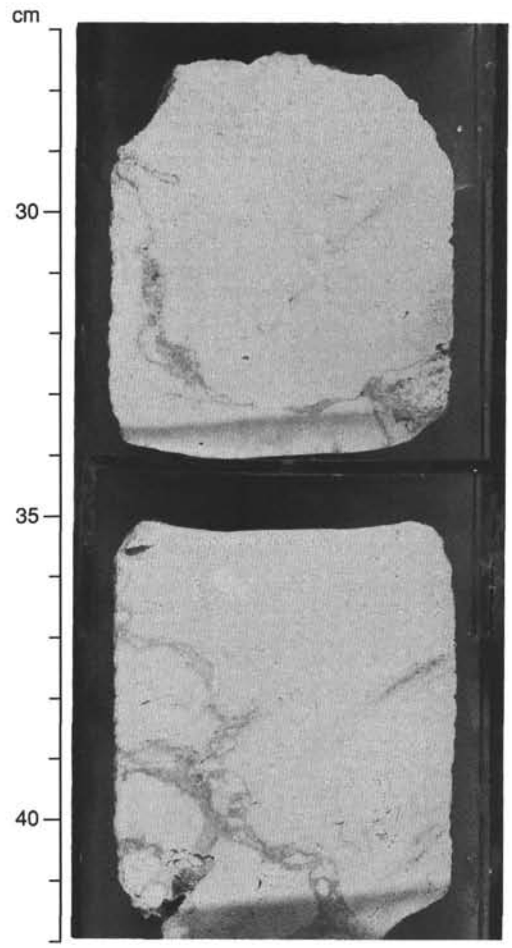

Figure 11. Fractures in biomicrite filled with secondary calcite (Section 160-965A-27X-1, 27–42 cm).

Subsidence of the land mass (seamount) or relative sea-level fall then took place and shallow hypersaline lakes, or marginal marine lagoons, developed in which dolomite and aragonite precipitated (lithostratigraphic Unit II). Minor relative sea-level regressions allowed the development of possible soils in some of these sediments prior to final drowning, as subsidence continued probably in the late Miocene or during the very earliest Pliocene.

Thereafter, as tectonic forces associated with plate margin tectonics in the region became more active, the carbonate sequence (together with the underlying "basement") was faulted as a series of blocks, which created a topography conducive to debris-flow deposition with talus fans developing along inferred fault scarps. These talus cones were possibly reworked to form a relatively flat(?) topography near paleo-sea level.

The nature of the tectonic subsidence is not known, but several possibilities can account for the discontinuous nature of the succession of fine-grained deep-water calcareous sediments of lithostratigraphic Unit I: (1) subsidence took place as a series of "pulses" with periods of inactivity when accumulation occurred; (2) subsidence was continuous and rapid with uninterrupted sedimentation, and missing portions of the section slumped as the accumulating pile became unstable; or (3) subsidence took place only later, followed by large-scale intraformational slumping of the entire sequence. Considering the geographic setting from which the section was recovered, option 2 is the most likely.

BIOSTRATIGRAPHY AND SEDIMENTATION RATES

Calcareous Nannofossils

Calcareous nannofossils were studied in all core-catcher samples that contained sediment or lightly lithified rock. Because many of the biozones could not be detected using only the core catchers, additional samples were collected from within the cores.

The calcareous nannofossil biostratigraphy at Site 965 is typified by assemblages that range from Pleistocene through early Pliocene age. Calcareous nannofossils are abundant or common in all of the Pleistocene samples, but decrease to common or few in the Pliocene material. Preservation is very good for the Pleistocene age samples and diminishes to fair in the Pliocene samples. A paucity of nannofossils prevented shipboard determination of the ages of samples from the bottom of each hole. Reworking was minimal and did not hinder the recognition of biozones. A summary of the biostratigraphy is described below and displayed in Figure 15.

Samples 160-965A-1H-1, 4 cm, through 1H-CC are in Zone MNN21 and contain *Emiliania huxleyi*. The accompanying assemblage includes small *Gephyrocapsa* (<3.5 μm), *Gephyrocapsa oce-*

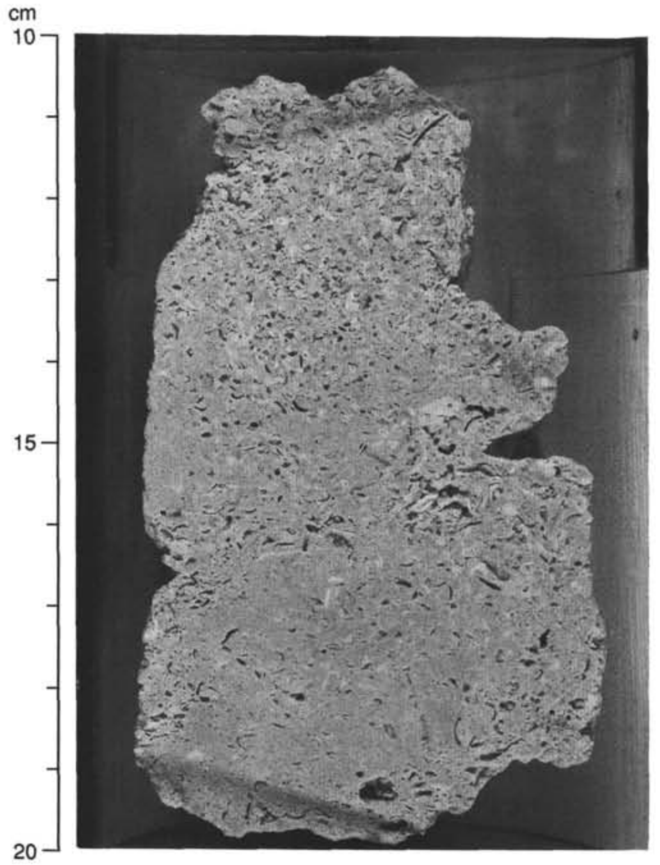

Figure 12. Biosparite cemented by calcite showing both vuggy and moldic porosity (Section 160-965A-10X-1, 10–20 cm).

Table 2. Dominant composition of thin sections of limestone from Site 965.

Core, section	Depth (mbsf)	Component (dominant)	Texture
160-965A-			
5X-1	29	Ooids	Grainstone
6X-1	31	Ooids	Grainstone
8X-1	58	Foraminifers/mollusks	Grainstone/packstone
10X-1	77	Mollusks/foraminifers	Grainstone/packstone
12X-1	97	Ooids/algae	Packstone
13X-1	106	Algae	Wackestone
19X-1	164	Foraminifers	Grainstone
21X-1	184	Algae	Wackestone
26X-1	232	Bioclasts/algae	Wackestone
27X-1	240	Algae	Wackestone (fractured)

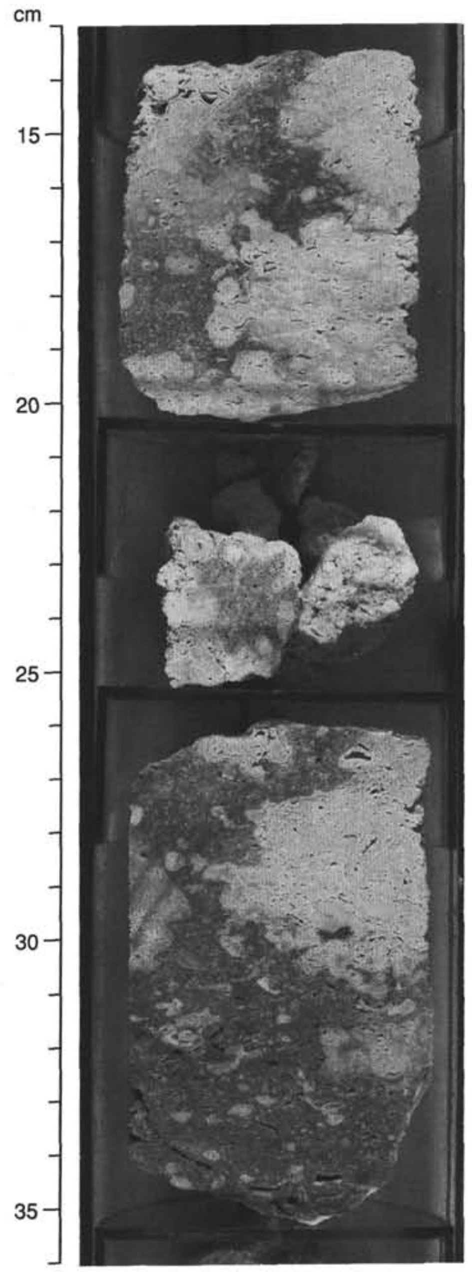

Figure 13. Algal wackestone with large oncolites in a softer dark micrite matrix (Section 160-965A-21X-1, 13–36 cm).

anica s.l., *Helicosphaera kamptneri, Coccolithus pelagicus, Rhabdosphaera clavigera,* and *Pontosphaera japonica.* The acme of *E. huxleyi* was not identified.

Samples 160-965A-2H-1, 8 cm, through 2H-2, 133 cm, were placed in Zone MNN20, which is a gap zone defined by the absence of both *E. huxleyi* and *Pseudoemiliania lacunosa.* The accompanying assemblage is similar to that found uphole.

Samples 160-965A-2H-3, 9 cm, through 2H-4, 104 cm, contain nannofossils from Zone MNN19f. The upper boundary of the zone is defined by the last occurrence of *P. lacunosa,* whereas the lower boundary is defined by the first occurrence of *Gephyrocapsa* sp. 3.

Samples 160-965A-2H-4, 126 cm, through 2H-7, 8 cm, contain nannofossils from Zone MNN19e. This interval is interpreted as a gap zone identified by the absence of both *Gephyrocapsa* sp. 3 and large *Gephyrocapsa* (>5.5 μm). The large *Gephyrocapsa* (>5.5 μm) last occurrence was used as a marker for the base of this zone. Small *Gephyrocapsa* and *P. lacunosa* dominate the accompanying assemblage.

Samples 160-965A-2H-7, 30 cm, through 2H-CC contain nannofossils from Zone MNN19d. This zone is identified by the presence of large *Gephyrocapsa* (>5.5 μm). The accompanying assemblage is dominated by small *Gephyrocapsa, P. lacunosa,* and *G. oceanica* s.l. and is similar to that found uphole.

The assemblage from Samples 160-965A-3H-1, 20 cm, through 3H-3, 70 cm, contains *Discoaster brouweri* and other species associated with Zone MNN18. This assemblage suggests that an unconformity exists between Samples 160-965A-2H-CC and 3H-1, 20 cm. The missing interval includes calcareous nannofossil Zones MNN19c–MNN19a. The accompanying assemblage includes small *Gephyrocapsa, Calcidiscus macintyrei, H. kamptneri, Helicosphaera sellii,* and *Syracosphaera pulchra.*

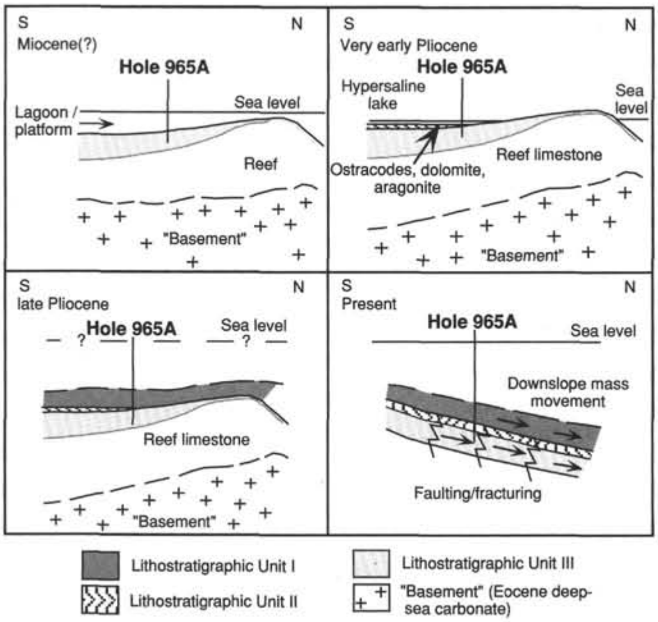

Figure 14. Conceptual model of the depositional and related tectonic events reconstructed from the sedimentary sequence recovered at Site 965. (Not to scale; depth to "basement" is several kilometers, and horizontal distances could be tens of kilometers.)

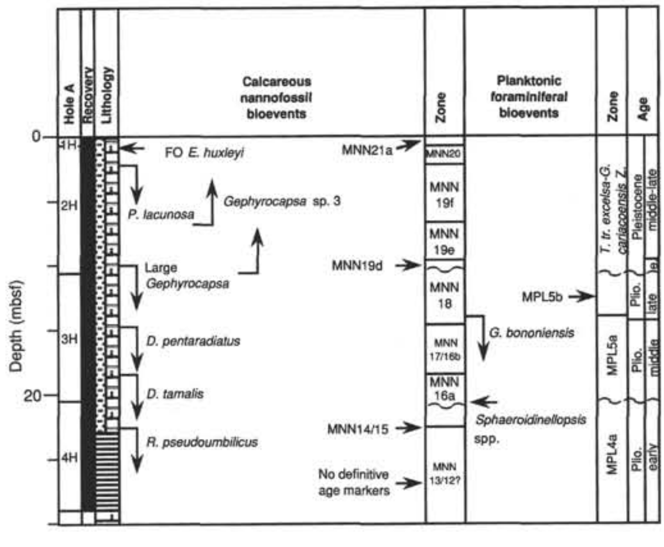

Figure 15. Composite of biostratigraphic events recognized at Site 965 including the lithostratigraphic record.

In Samples 160-965A-3H-4, 20 cm, through 3H-6, 20 cm, *Discoaster pentaradiatus* and *Discoaster surculus* become a significant part of the assemblage. Therefore, these samples are placed in Zones MNN17–16b. *Discoaster brouweri, Discoaster intercalaris, Discoaster asymmetricus,* and rare occurrences of *Discoaster triradiatus* typify the accompanying assemblage.

The top of Zone MNN16a is identified by the last common occurrence of *Discoaster tamalis* and is recognized in Samples 160-965A-3H-6, 80 cm, through 3H-7, 65 cm. Beginning in Sample 160-965A-4H-1, 20 cm, *D. pentaradiatus* disappears from the assemblage. An interval of "paracme" of *D. pentaradiatus* reported by Rio et al. (1990) from the lowermost part of Zone MNN16a to the uppermost part of Zone MNN14–15 is considered useful for very fine biostratigraphic subdivision. This peculiar distribution of *D. pentaradiatus* in the Mediterranean Pliocene marine record was reported for the first time by Driever (1981). According to Channell et al. (1992) and Sprovieri (1993), this paracme interval begins at 3.90 Ma very close to the *Globorotalia margaritae* last common occurrence, and ends at 3.56 Ma, close to the *Globorotalia puncticulata* last occurrence. In Hole 965A the top of the *D. pentaradiatus* paracme coincides with an unconformity recognized by a missing foraminiferal zone (see planktonic foraminifer discussion below). The accompanying assemblage is similar to that found in the preceding sample.

Samples 160-965A-4H-2, 125 cm, through 4H-3, 54 cm, contain nannofossils belonging to Zones MNN14–15. These zones contain both *Reticulofenestra pseudoumbilicus* (>7 µm) and common specimens of *D. asymmetricus.* The accompanying in situ assemblage is dominated by discoasters similar to those found uphole.

The interval from Samples 160-965A-4H-3, 125 cm, through 4H-CC could not be confidently placed into a biozone because of poor preservation and a paucity of calcareous nannofossils. The assemblage includes rare overgrown discoasters that appear to be Neogene in age. Sample 160-965A-4H-CC contained rare *Amaurolithus delicatus,* which suggests that this sample is lower Pliocene (MNN13 Zone) to upper Miocene (*Calcidiscus leptoporus* Zone). Reworking is heavy in the entire assemblage and consists of overgrown or partially dissolved Paleogene specimens of *Ericsonia formosa, Discoaster saipanensis, Cylicargolithus floridanus,* and medium-sized species of *Dictyococcites.*

Planktonic Foraminifers

Hole 965A was studied in detail in order to provide a complete stratigraphic record of the sedimentary sequence. Four core-catcher samples and 15 additional samples were analyzed for planktonic foraminiferal content.

The Pliocene planktonic foraminiferal assemblages do not display significant differences from the previous sites drilled during Leg 160. Planktonic foraminifers range in abundance from rare to dominant at Site 965 and consist of diversified and poorly to well-preserved Pleistocene and Pliocene faunas. Using the zonation scheme of Cita (1975), emended by Sprovieri (1993), the interval spanning the *Truncorotalia truncatulinoides excelsa–Globigerina cariacoensis* Zones was identified for the Pleistocene and three zonal boundaries were identified for the Pliocene that encompass Zones MPL4a through MPL5b.

As observed at Sites 963 and 965, the zonal boundary between the *T. truncatulinoides excelsa* and *G. cariacoensis* Zones was not recognized owing to the scarcity of *T. truncatulinoides excelsa.* The two zones span the entire Pleistocene, from Samples 160-965A-1H-1, 33–34 cm, through 2H-6, 131–132 cm. Faunal assemblages are generally well preserved and abundant and very similar to those observed for Sites 963 and 965.

Pliocene Zone MPL6 was not recognized, suggesting a depositional hiatus between the lower Pleistocene and upper Pliocene in Hole 965A. Sample 160-965A-2H-CC was assigned to Zone MPL5b as it contains the highest occurrence of the Pliocene taxa *Globigerinoides obliquus* and is devoid of *Globorotalia inflata,* the lowest occurrence of which would normally mark the base of Zone MPL6.

Zone MPL5a was identified from Samples 160-965A-3H-4, 17–19 cm, through 3H-CC. It is recognized by the last occurrence of *Globorotalia bononiensis* and the absence of *Sphaeroidinellopsis* spp.

Samples 160-965A-4H-1, 95–97 cm, through 4H-CC contain *Sphaeroidinellopsis* spp. and *Globorotalia puncticulata.* This assemblage marks Zone MPL4a, which indicates that Zone MPL4b is not represented in the sampled intervals.

The highest occurrence of *G. puncticulata,* in Sample 160-965A-4H-1, 95–97 cm, marks the top of MPL4a.

Reworking has not severely affected the planktonic foraminiferal assemblages, and no "older" species were observed in this hole. However, many specimens display clearly different degrees of preservation and they may not all be in place. Therefore, a paleoenvironmental interpretation is hampered at Hole 965A.

Other Taxa

Only very few specimens of Bolboforma were found in the samples from Hole 965A. They occur in Samples 160-965A-2H-4, 9–11 cm, 3H-1, 69–71 cm, and 3H-3, 17–19 cm (lower Pliocene); they may possibly be attributed to *Bolboforma* sp. E (Spiegler and Rögl, 1992).

The carbonate sequence located between Cores 160-965A-5X and 27X was not studied in detail aboard ship. However, sedimentological descriptions of these cores indicate the presence of corals, bivalves, echinoderms, calcareous algae, and benthic foraminifers (see "Lithostratigraphy" section, this chapter).

Approximately 30 thin sections were examined for microfossils. Samples 160-965A-8X-1, 10–16 cm, 10X-1, 11–14 cm, 23X-1, 51–57 cm, 24X-1, 34–37 cm, 24X-1, 55–61 cm, and 26X-1, 25–28 cm, contain abundant fragments of calcareous algae, some of which are tentatively attributed to the genus *Lithothamnium*. Abundant benthic foraminifers, mostly shallow-water miliolids and rare *Spiroplectammina* sp., were found throughout the sequence. Benthic foraminifers are more abundant in Samples 160-965A-26X-1, 25–28 cm, and 26X-1, 77–84 cm; however, these forms are not age diagnostic.

Sedimentation Rates

Sedimentation rates for Hole 965A were estimated using calcareous nannofossil and planktonic foraminiferal events from Hole 965A (Table 3). The data are plotted on the age vs. depth curve shown in Figure 16. An error line (dashed) is shown on the figure to indicate the degree of uncertainty as to the location of the nannofossil and foraminiferal events within this core. Intervals representing depositional hiatuses are also indicated on this figure.

Sedimentation rates vary from 0.05 to 16 m/m.y. throughout the sequence. Ten significant shifts in sedimentation rates were determined from the Site 965 data. From the seafloor to the first occurrence of *E. huxleyi* (0.26 Ma) the sedimentation rate was approximately 3 m/m.y. Sedimentation rates peaked to 16 m/m.y. in the interval from the first occurrence of *E. huxleyi* to the last occurrence of *P. lacunosa* (at 0.46 Ma). Sedimentation declined to 5 m/m.y. in the interval from *P. lacunosa* to the first occurrence of *Gephyrocapsa* sp. 3 at 0.99 Ma. In the interval between the latter bioevent and the last occurrence of large *Gephyrocapsa* (1.25 Ma) the sedimentation rate increased to about 15 m/m.y. In the interval marked by the last and first occurrence of large *Gephyrocapsa* (1.5 Ma) the sedimentation rate averaged 3 m/m.y. The next observed datum is the last occurrence of *G. bononiensis* (2.45 Ma), representing a time interval of 0.95 m.y. over approximately 0.2 m of sediment. The absence of five fossil datums that normally occur within this interval indicates that the section between the first occurrence of large *Gephyrocapsa* (1.5 Ma) and the last occurrence of *G. bononiensis* represents a depositional hiatus. From the last occurrence of *G. bononiensis* to the last occurrence of *D. pentaradiatus* (1.99 Ma) sedimentation rates averaged about 0.05 m/m.y. From the last occurrence of *D. pentaradiatus* to the last occurrence of *D. tamalis* (2.82 Ma) sedimentation rates were approximately 12 m/m.y. The next observed datum is the last occurrence of *G. puncticulata* (3.57 Ma), spanning a time interval of up to 0.75 m.y. over a 0.5-m interval. The absence of the *Sphaeroidinellopsis* spp. last occurrence indicates that the interval between the last common occurrence of *D. tamalis* (2.82 Ma) and the first occurrence of *G. puncticulata* (3.57 Ma) represents a depositional hiatus of up to 0.75 m.y. From the first occurrence of *G. puncticulata* down to the bottom of the hole (last occurrence of *R. pseudoumbilicus* at 3.85 Ma) sedimentation rates averaged 7 m/m.y.

Table 3. Stratigraphic list of calcareous nannofossil and planktonic foraminifer events for Site 965.

Event	Core, section, interval (cm)	Depth (mbsf)	Age (Ma)
	160-965A-		
FO *E. huxleyi**	1H-CC	0.76	0.26
LO *P. lacunosa*	2H-3, 9	3.89	0.46
FO *Gephyrocapsa* sp. 3	2H-4, 104	6.34	0.99
LO *Gephyrocapsa* >5.5 µm	2H-7, 30	10.10	1.25
FO *Gephyrocapsa* >5.5 µm	2H-CC	10.78	1.5
LO *G. bononiensis*	3H-4, 17–19	14.99	2.45
LO *D. pentaradiatus*	3H-4, 20	15.00	2.51
LCO *D. tamalis*	3H-6, 80	18.60	2.82
LO *R. pseudoumbilicus*	4H-2, 125	22.55	3.85

Notes: FO = first occurrence; LO = last occurrence; LCO = last common occurrence; * = to be confirmed by scanning electron microscopy.

PALEOMAGNETISM

Paleomagnetic measurements were restricted to the upper 24 m of Hole 965A (i.e., to the bottom of Core 160-965A-4H), the interval in which sediment recovery was essentially continuous. Below this stratigraphic level, recovery was low and no oriented material was retrieved. Paleomagnetic measurements at Site 965 were routinely made on the archive halves of each core section at 10-cm intervals after AF demagnetization at 20 mT. NRM intensities were well above the noise level of the magnetometer in the upper 24 m of Hole 965A (Fig. 17). Both the NRM intensity and the low-field magnetic susceptibility display large variations (Fig. 17). These variations may be re-

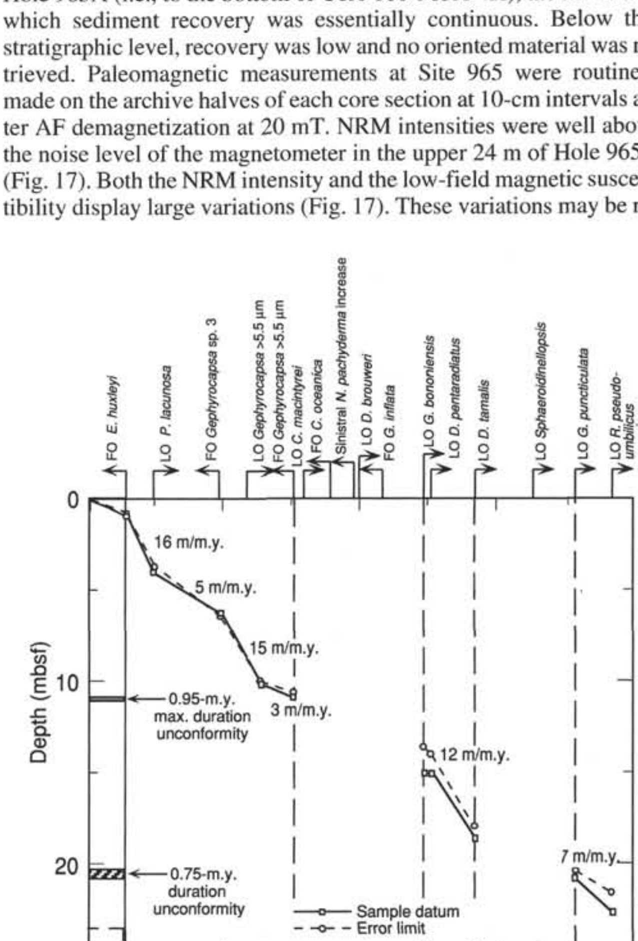

Figure 16. Age vs. depth diagram showing selected calcareous nannofossil and planktonic foraminifer datums with corresponding sedimentation rates. The solid line (connecting squares) corresponds to the last sample where the marker species was found for the corresponding first or last occurrence datum; the dashed line (connecting circles) corresponds to the nearest sample where the marker species was not found. The vertical dashed lines indicate the maximum time ranges of the corresponding depositional hiatuses.

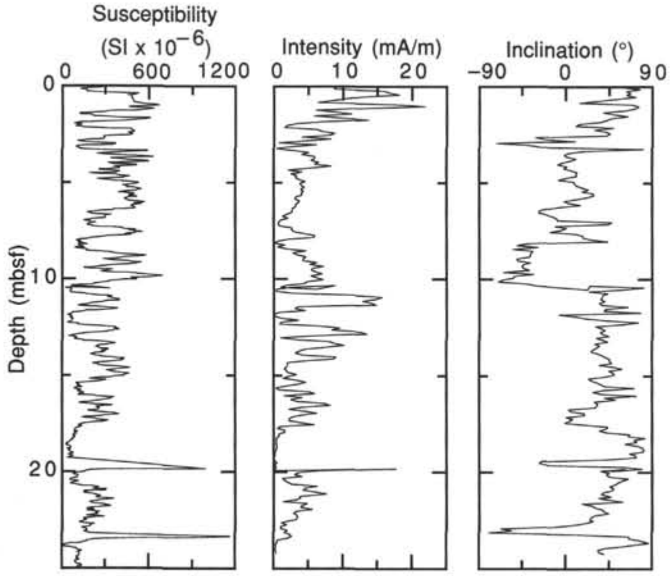

Figure 17. Magnetic susceptibility, NRM intensity, and inclination after AF demagnetization at 20 mT for Hole 965A.

lated to lithologic changes that are interpreted to result from debris flows and other types of downslope mass movement (see "Lithostratigraphy" and "Structural Geology" sections, this chapter). The whole-core log of demagnetized inclination for Hole 965A is shown in Figure 17. Several intervals of normal and reverse polarity are evident, but it is not possible to make an unambiguous interpretation of the data for several reasons. First, the chaotic nature in which the sediments were deposited suggests that they are not ideal for paleomagnetic studies. Second, variable degrees of normal polarity overprinting, including Brunhes Chron overprinting and likely contamination by strong fields within the drill string, are evident in sediments recovered from other sites during Leg 160. The unknown extent of normal polarity overprinting means that the whole-core data may be insufficiently reliable for polarity interpretation in these sediments. Third, paleontological data indicate that the sequence includes at least two hiatuses (see "Biostratigraphy and Sedimentation Rates" section, this chapter). Discrete samples were not taken because of the nonideal nature of these sediments; therefore, the paleomagnetic behavior could not be elucidated at Hole 965A.

Despite the above-mentioned uncertainties and the unconfirmed nature of the paleomagnetic record at Hole 965A, some general trends can be drawn from the inclination data shown in Figure 17. First, the record is unclear from 0 to 8 mbsf. Second, a zone of reversed polarity is evident from 8 to 10 mbsf. Paleontological data indicate that a hiatus that spans the interval from 1.5 to 2.45 Ma occurs between 10.8 and 11.0 mbsf (see "Biostratigraphy and Sedimentation Rates" section, this chapter). The zone of reversed polarity from 8 to 10 mbsf may therefore represent part of the middle Matuyama Chron, between the Jaramillo and Olduvai Subchrons. Third, the zone of normal polarity below 11 mbsf may represent part of the upper Gauss Chron. Fourth, paleontological data indicate the presence of another hiatus at about 20 mbsf that represents the interval from about 2.8 to 3.6 Ma (see "Biostratigraphy and Sedimentation Rates" section, this chapter). It is therefore not possible to place any other chronological constraints using the presently available paleomagnetic data. Inclination features from the lower part of the record cannot be interpreted unambiguously because of the lack of a clear stratigraphic framework resulting from the presence of a hiatus at about 20 mbsf and a probable paleosol at 23.2 mbsf (see "Lithostratigraphy" section, this chapter).

STRUCTURAL GEOLOGY

Structural features are rare and occur almost entirely in the semilithified sediments of Core 160-965A-3H. The fragmentation of the carbonate into angular blocks (up to 7 cm in length) was caused by RCB and XCB drilling processes on layered sediments with contrasting rheology.

The upper part of the succession shows planar changes in color and grain size on a centimeter to decimeter scale that represent sedimentary bedding. These have consistently horizontal to subhorizontal orientations. Other features—such as faint laminations and thin dark-gray to black layers and patches (pyrite or monosulfide enrichment and volcanic ash deposits)—are also generally oriented horizontally with respect to the core coordinates. Rarely, bedding planes dip up to 30° (cf., Sections 160-965A-2H-2 and 2H-3); these are interpreted as related to slump processes ("Lithostratigraphy" section, this chapter).

The sporadic normal microfaults in the unconsolidated nannofossil oozes that were observed in Cores 160-965A-1H through 4H are most common in Core 160-965A-3H, where they are associated with the tilted beds (described above) and debris flows. Moderate to steep dips and offsets along curviplanar surfaces ranging from a few millimeters up to 1.5 cm were found (Table 4, Fig. 18). Offsets of some faults that could not be measured were estimated to be more than 5 cm. The data set is too small for a thorough interpretation. However, it may be significant that the strike of the planes with respect to core coordinate (Fig. 19) is similar to that observed at Site 964 and that therefore, the origin of these features may be either tectonic or drilling induced.

Poor core recovery and fragmentation of carbonates below Core 160-965A-4H excluded the measurement of structural features with respect to core coordinates. However, in thin section, angular carbonate clasts encrusted with algae (Core 160-965A-26X and below) are cemented with secondary calcite. This texture is more common with increasing depth and suggests that a brecciation event was followed by diagenetic fluid flux and cementation.

Tensor data were obtained only for Core 160-965A-4H. Reorientation of structural features other than the horizontal bedding planes in this core to geographic coordinates was, therefore, not possible.

The association of microfaults, slumped beds, and debris flows in Cores 160-965A-2H and 3H suggests that the facies and structural features may be related to sediment transport downslope, in conjunction with tectonic faulting. This interpretation is supported by paleontological evidence that suggests that there are two hiatuses in the sequence between the bottom of Core 160-965A-2H and the top of Core 160-965A-4H (Fig. 16, "Biostratigraphy and Sedimentation Rates" section, this chapter). Site 965 is positioned on a narrow, north-south-trending ridge on the northern flank of the Eratosthenes Seamount (cf., Figs. 4, 5, "Geological Setting" section, this chapter). It is bounded by steep, northeastward- and southwestward-dipping normal faults that are identified in seismic records (Limonov and Woodside, 1994). Faulting and slumping observed in the upper part of the succession were probably caused by extensional activity along these lineaments. Similar faulting is also likely to have caused the brecciation of the carbonates.

ORGANIC GEOCHEMISTRY

Volatile Hydrocarbons

As part of the shipboard safety and pollution-prevention monitoring program, hydrocarbon gases were analyzed in each core of Hole 965A by the headspace technique while drilling in soft sediment and in approximately every second core in consolidated carbonates. Only trace concentrations of methane in the range of 2 to 6 ppm were recorded.

Table 4. Structural data collected at Site 965.

Core, section, interval (cm)	Depth (mbsf)	Feature	Offset width (cm)	Orientation on core face (degrees) Apparent dip	Direction	Second apparent orientation (degrees) Apparent dip	Direction	Calculated orientation (degrees) Dip	Direction	Comments
160-965A-										
3H-1, 7–15	10.37	F	1	48	90	0	320	55	50	Normal fault
3H-2, 24–27	12.04	F		61	90	0	340	62	70	Normal fault(?)
3H-2, 32–40	12.12	F		42	90	20	180	44	112	Normal fault
3H-2, 41–67	12.21	F	1.5	77	90	0	345	77	75	Normal fault
3H-3, 2–9	13.32	F	0.5	40	90	0	350	40	80	Normal fault
3H-3, 28–43	13.58	F		63	270	0	20	69	290	Vein/fracture/fluid-escape structure, color change
3H-7, 5–9	19.35	SB		32	270	5	0	32	278	Bedding

Note: Feature symbols defined in Table 2 ("Explanatory Notes" chapter, this volume).

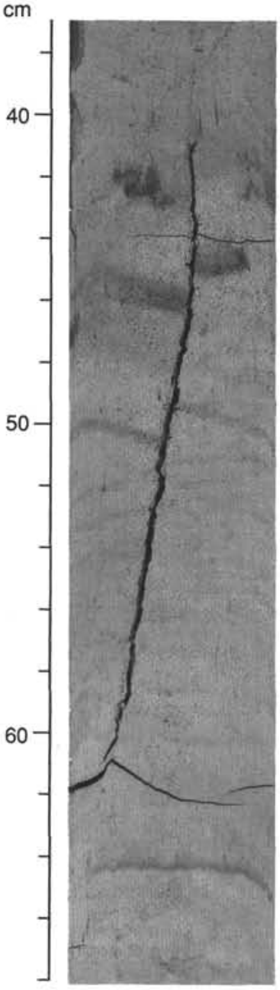

Figure 18. Normal microfaults in Section 160-965A-3H-2, 15–70 cm. Note the approximately 1.5-cm offset of dark-gray pyritic layers between 44.5 and 46 cm and between 49 and 50.5 cm along a steep fault plane. A shallower dipping microfault crosses the section from 35 to 45 cm. The crack down the center of the core appeared after core splitting, but follows the orientation of the fault measured.

Carbon, Nitrogen, and Sulfur

The abundances of total, inorganic, and organic carbon, calcium carbonate, and total nitrogen and sulfur in soft sediments from Hole 965A are summarized in Table 5. Random sampling was performed for Hole 965A, with additional samples taken from the sapropels.

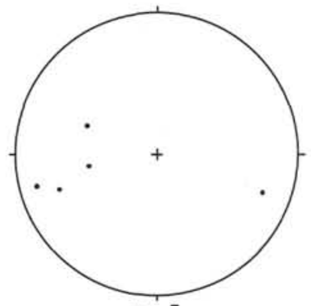

Figure 19. Equal-area lower hemisphere projection of poles to normal faults with respect to the core reference frame.

Carbonate contents are variable but are mostly close to or >40% (Table 5). Organic carbon concentrations are low (<0.5%) in the background sediments but range from 1.40% to 4.72% in the sapropels. This variation is at least partly due to secondary alteration by benthic activity. C_{org}/N ratios for sediments rich in organic matter are significantly above 10 (Table 5) and, thus, are in the range determined for sapropels at Site 964. They are not suitable for distinguishing marine from terrigenous organic matter. Sulfur content is low at Site 965 compared to the high values recovered for the sapropels at Site 964 (see "Organic Geochemistry" section, "Site 964" chapter, this volume).

Rock-Eval Pyrolysis

Rock-Eval pyrolysis was performed for selected organic-carbon-rich intervals from Hole 965A (Table 6). Hydrogen index values exceed 150 only in the sapropels containing more than 2% organic carbon. The HI values together with the high oxygen index values suggest the presence of mixed marine and terrigenous organic matter. Because aerobic secondary alteration has probably also lowered the hydrogen content of the marine organic matter, it is difficult to reliably estimate the relative proportions of marine and terrigenous organic matter. The temperatures of maximum pyrolysis yield (T_{max}) are relatively high (>420°C) for the shallow setting and young age of the sediments, which corroborates the presence of (partly) oxidized organic matter.

PHYSICAL PROPERTIES

Physical properties were measured in all whole-round APC-recovered sections (Cores 160-965A-1H through 4H), excluding core catchers, using the MST, which comprises the GRAPE, *P*-wave velocity logger, natural gamma-ray device, and magnetic susceptibility

Table 5. Concentration of total, inorganic, and organic carbon, calcium carbonate, total nitrogen, and sulfur in sediments from Hole 965A.

Core, section, interval (cm)	Depth (mbsf)	Total carbon (%)	Inorganic carbon (%)	Organic carbon (%)	$CaCO_3$ (%)	Nitrogen (%)	Sulfur (%)	C_{org}/N	C_{org}/S
160-965A-									
1H-1, 9–10	0.09	7.13	6.99	0.14	58.23	0.02	0.08	7.2	1.8
1H-1, 39–40	0.39	6.21	5.94	0.27	49.48	0.03	0.09	8.9	3.0
1H-CC, 2–3	0.58		7.20		59.98				
2H-1, 27–28	1.07		6.17		51.40				
2H-1, 64–65	1.44	6.18	4.54	1.64	37.82	0.12	1.30	13.7	1.3
2H-2, 50–51	2.80	7.27	5.87	1.40	48.90	0.09	0.19	15.6	7.3
2H-3, 69–70	4.49		5.96		49.65				
2H-5, 69–70	7.49		5.77		48.06				
2H-7, 55–56	10.35	8.74	4.02	4.72	33.49	0.28	1.66	17.0	2.8
2H-7, 61–62	10.41	6.05	5.57	0.48	46.40	0.04	0.52	12.0	0.9
3H-1, 13–14	10.43	8.30	5.47	2.83	45.57	0.14	0.23	19.8	12.5
3H-3, 59–60	13.89		8.53		71.05				
3H-5, 60–61	16.90		7.58		63.14				
3H-6, 70–71	18.50	10.24	6.90	3.34	57.48	4.35	0.89	0.8	3.7
4H-3, 70–71	23.50		3.14		26.16				
4H-5, 70–71	26.50		4.73		39.40				

Table 6. Results of Rock-Eval pyrolysis for Hole 965A.

Core, section, interval (cm)	Depth (mbsf)	S_1 (mg/g)	S_2 (mg/g)	S_3 (mg/g)	TOC	PC	HI	OI	T_{max} (°C)	PI	S_2/S_3
160-965A-											
2H-1, 64–65	1.44	0.40	1.66	3.70	1.64	0.17	101	225	421	0.19	0.44
2H-2, 50–51	2.80	0.30	1.40	3.06	1.40	0.14	100	218	423	0.18	0.45
2H-7, 55–56	10.35	1.26	11.22	5.09	4.72	1.04	237	107	424	0.10	2.20
3H-1, 13–14	10.43	0.76	9.30	4.22	2.83	0.83	328	149	430	0.08	2.20
3H-6, 70–71	18.50	0.52	5.38	3.33	3.34	0.49	161	99	426	0.09	1.61

Notes: TOC = total organic carbon; PC = petroleum potential as pyrolyzable carbon; HI = hydrogen index; OI = oxygen index; PI = production index; see the "Explanatory Notes" chapter (this volume) for these parameters.

meter. Thermal conductivity was also measured in these sections. Vane shear strength and compressional wave velocity were measured in split APC core sections from Hole 965A (see "Explanatory Notes" chapter, this volume, for technical details of these procedures). Recovery in XCB Cores 160-965A-5X through 27X was too poor to measure them with the MST, digital sonic velocimeter system, or thermal conductivity needle-probe method. A suite of physical index property measurements was performed on samples from each split APC core section and sample pieces from nearly each XCB-recovered core; these measurements included dry- and wet-bulk density, grain density, porosity, water content, and void ratio. The results are listed in Tables 7 through 10, and are shown graphically in Figures 20 through 25. In this section, we describe the downhole distribution of selected physical properties of Hole 965A.

Index Properties

The measured index properties include measurements of mass and volume of selected sediment samples, from which water content, bulk and dry density, bulk and dry porosity, void ratio, and grain density were calculated (Table 7). The XCB samples may have lost some of their water content before they were measured. They were not resaturated for the measurements, but kept in closed boxes with a saturated sponge for several hours.

Bulk density values show a steady increase from approximately 1.6 to 1.8 g/cm^3 in the upper 24 mbsf and then a steplike increase to values of about 1.9 g/cm^3 (Fig. 20). Below that depth, XCB cores yielded hard rocks with low core recovery, so that the true depth of the samples may be up to 9 m deeper. The density of the hard rocks varies between 2.3 and 2.7 g/cm^3. Water content, expressed relative to dry weight, varies from more than 40 wt% just below the seafloor to less than 25 wt% (Fig. 20) and the porosity decreases from more than 70 to 35 vol% (Fig. 20) for the oozes to a depth of 39 mbsf, with a sharp decrease at 24 mbsf. The measured water content and porosity for the carbonate rocks below 39 mbsf may be underdetermined because the samples partly dried before they were measured. This is indicated by three results with apparently zero porosity.

GRAPE Density

The wet-bulk density from GRAPE measurements (Fig. 21A) shows an overall increase with depth in Hole 965A, with large increases between 0 and 2 mbsf and between 20 and 24 mbsf. A comparison of GRAPE density with the wet-bulk density index property (Fig. 21) shows general agreement between the two methods, although GRAPE density values are generally lower than the index property bulk density. This is most likely because the GRAPE density was measured in undrained whole-round cores in their liners, which have a higher water content than discrete index properties samples taken from split cores.

Compressional Wave Velocities

Compressional wave velocity was measured parallel and normal (Table 8, Fig. 22A) to the core axis on split APC cores from Hole 965A using the DSV system. For XCB cores, five samples were cut to obtain two parallel surfaces and the compressional wave velocity was measured parallel to the core axis. Velocities generally increase with depth, from about 1.55 km/s at the seafloor to 1.7 km/s at nearly 30 mbsf. A similar trend of velocity variation was measured in the MST, although the precision of these measurements is affected by measuring through the core liner (Fig. 22B). The increase of compressional wave velocity is stronger below 20 mbsf. The velocity patterns at Hole 965A are consistent with the other measured index properties discussed above; in particular, the downhole distribution of wet-bulk density is also reflected in the velocity.

Table 7. Index properties measured in cores from Hole 965A.

Core, section, interval (cm)	Depth (mbsf)	Water content (wt%)	Porosity (vol%)	Bulk density (g/cm^3)		Grain density (g/cm^3)		Dry density (g/cm^3)	
				Method B	Method C	Method B	Method C	Method B	Method C
160-965A-									
1H-1, 35–37	0.35	44.33	79.64	1.62	1.57	3.00	2.74	0.90	0.88
2H-1, 47–49	1.27	43.20	76.05	1.65	1.59	3.09	2.73	0.94	0.90
2H-1, 98–100	1.78	32.81	48.84	1.84	1.78	3.03	2.76	1.24	1.19
2H-2, 38–40	2.68	43.15	75.90	1.62	1.59	2.91	2.75	0.92	0.91
2H-2, 117–119	3.47	36.22	56.78	1.74	1.70	2.88	2.72	1.11	1.09
2H-3, 44–46	4.24	36.09	56.46	1.74	1.70	2.88	2.72	1.11	1.09
2H-3, 107–109	4.87	38.04	61.39	1.74	1.66	3.03	2.69	1.08	1.03
2H-4, 37–39	5.67	35.87	55.93	1.80	1.72	3.14	2.78	1.16	1.10
2H-4, 98–100	6.28	34.44	52.54	1.82	1.75	3.06	2.77	1.19	1.14
2H-5, 37–39	7.17	36.45	57.35	1.79	1.71	3.11	2.76	1.14	1.08
2H-5, 100–102	7.80	10.45	11.67	1.68	2.32	1.82	2.72	1.51	2.08

Only part of this table is reproduced here. The entire table appears on the CD-ROM (back pocket).

Table 8. Compressional wave velocity measured in APC cores from Hole 965A.

Core, section, interval (cm)	Depth (mbsf)	Measurement type	Velocity (km/s)
160-965A-			
1H-1, 3	0.03	DSV 1	1.544
1H-1, 3.5	0.04	DSV 2	1.569
2H-1, 7.2	0.87	DSV 1	1.531
2H-1, 8.4	0.89	DSV 2	1.529
2H-1, 62.1	1.42	DSV 1	1.577
2H-1, 62	1.42	DSV 2	1.639
2H-2, 81.9	3.12	DSV 2	1.57
2H-2, 4.6	2.35	DSV 1	1.582
2H-2, 5.2	2.35	DSV 2	1.596
2H-3, 69.8	4.50	DSV 1	1.631

Note: Direct DSV measurements.

Only part of this table is reproduced here. The entire table appears on the CD-ROM (back pocket).

Table 9. Vane shear strength measured in split APC cores from Hole 965A.

Core, section, interval (cm)	Depth (mbsf)	Strength (kPa)
160-965A-		
1H-1, 4.2	0.04	7.5
2H-1, 7.1	0.87	10.6
2H-1, 62.2	1.42	12.1
2H-2, 4.1	2.34	16.2
2H-2, 81.1	3.11	17.8
2H-3, 8.8	3.89	17.8
2H-3, 70.1	4.50	20.2
2H-4, 3.2	5.33	18.0
2H-4, 63.1	5.93	27.6
2H-5, 0.4	6.80	27.8

Only part of this table is reproduced here. The entire table appears on the CD-ROM (back pocket).

Shear Strength

Measurements of shear strength, using a mechanical vane, were made on split APC cores from Hole 965A to a depth of 28 mbsf, concurrent with the measurement of compressional wave velocity. Values range approximately from 10 to 60 kPa, and generally increase with depth (Table 9, Fig. 22A). The decreasing water content with depth (Fig. 20) results in the higher shear strength and the correlation of vane shear with velocity.

Table 10. Thermal conductivity measured in split APC cores from Hole 965A.

Core, section, interval (cm)	Depth (mbsf)	Thermal conductivity (W/[m • K])
160-965A-		
1H-1, 30	0.30	1.04
2H-1, 50	1.30	1.16
2H-2, 50	2.80	1.31
2H-3, 50	4.30	1.09
2H-4, 50	5.80	1.18
2H-5, 50	7.30	1.29
2H-6, 50	8.80	1.25
2H-7, 30	10.10	1.21
3H-1, 50	10.80	1.26
3H-2, 50	12.30	1.21

Only part of this table is reproduced here. The entire table appears on the CD-ROM (back pocket).

Magnetic Susceptibility

Figure 23 shows the distribution of magnetic susceptibility with depth for APC cores from Hole 965A. The measurements show an increase from the seafloor to 5 mbsf, followed by a slow decrease in the magnetic susceptibility. Values range from 8×10^{-6} to 3×10^{-3} SI units.

Natural Gamma-ray Radiation

NGR values of APC cores from Hole 965A vary between 10 and 30 counts per second (cps) (Fig. 24). The peaks at 8–10 and 18–20 mbsf correlate with patterns observed in the other physical properties (e.g., bulk density in Fig. 20 and compressional wave velocity in Fig. 22A).

Thermal Conductivity

Thermal conductivity at Hole 965A was determined in every APC core section. The measurements show an overall increase from about 1.0 to 1.6 W/(m · K) (Table 10, Fig. 25) and do not reflect the fine stratification pattern in this borehole. The increase is interpreted as caused by compaction.

Relationship Between Physical Properties and Lithology

Clayey oozes that occur from the seafloor to 29 mbsf are the main constituent of the nonconsolidated part of Hole 965. The abrupt in-

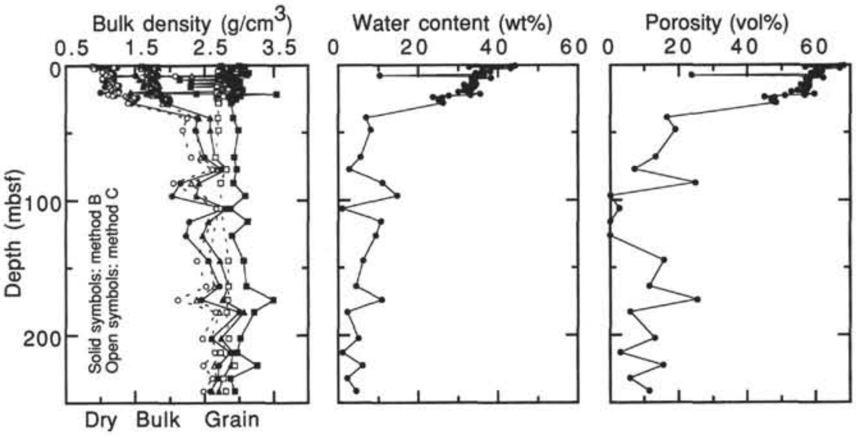

Figure 20. Index properties measured in cores from Hole 965A. Dry density = circles; bulk density = triangles; grain density = squares; Method B = filled symbols; Method C = open symbols.

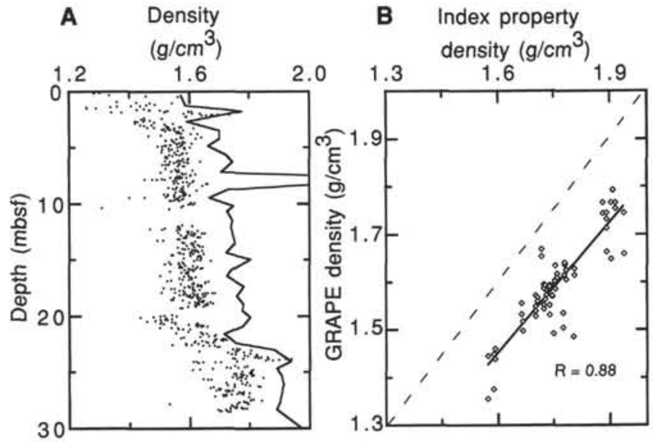

Figure 21. **A.** Bulk density measured with the GRAPE and from index property measurements (line). **B.** Comparison of density from index property and GRAPE measurements. R is the correlation coefficient and the solid line shows the linear regression.

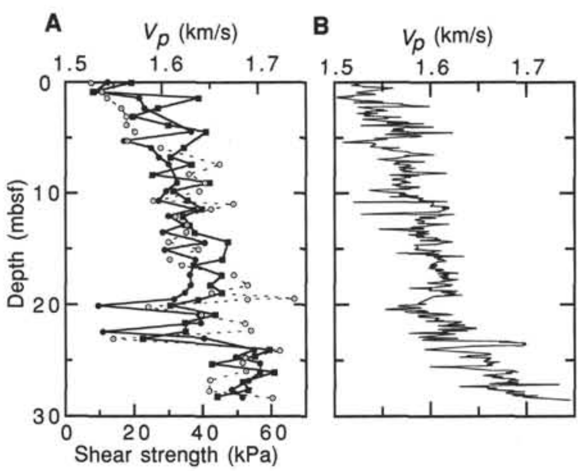

Figure 22. Compressional wave velocity and vane shear strength measured in cores from Hole 965A. **A.** Direct measurement in split cores; DSV 1 (parallel to core axis) = solid circles; DSV 2 (perpendicular to core axis) = solid squares; vane shear strength = open symbols. **B.** MST measurements through the liner of whole core sections (perpendicular to the core axis).

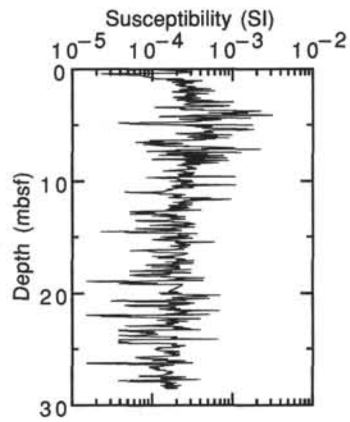

Figure 23. Magnetic susceptibility measured with the MST on cores from Hole 965A.

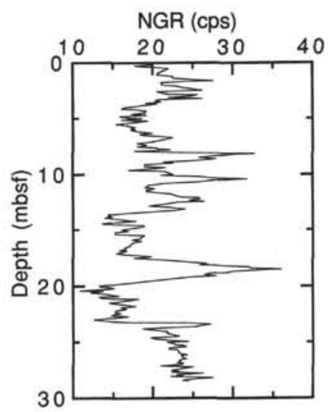

Figure 24. Natural gamma-ray radiation measured with the MST on cores from Hole 965A.

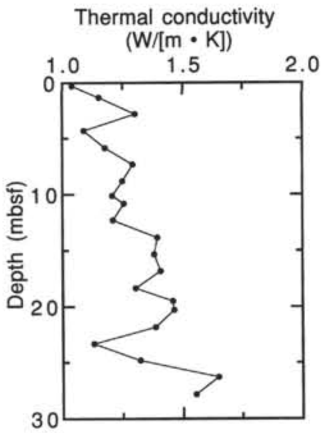

Figure 25. Thermal conductivity measured in cores from Hole 965A.

creases of bulk density, compressional wave velocity, and susceptibility in the upper 5 m of the hole indicate compaction. Based on the physical properties, the remaining section of oozes can be subdivided into three main units and three subunits (Table 11) that correlate with lithologic changes and stratigraphic events. A biostratigraphic hiatus, found at depth of 11–12 mbsf, where a large sequence from the middle Pleistocene to the upper Pliocene is apparently missing (see "Biostratigraphy and Sedimentation Rates" section, this chapter), is not expressed in the physical properties. At 20–23 mbsf, however, another hiatus occurs and the age of the sediment changes abruptly from middle Pliocene to early Pliocene (see "Biostratigraphy and Sedimentation Rates" section, this chapter); the change in MST velocity measurements (Fig. 22A) coincides with the biostratigraphic break. Owing to the poor core recovery between 29 and 250 mbsf (less that 5%) we can make only general statements for the recovered packstone/grainstone/mudstone section: the density is between 2.4 and 2.7 g/cm^3 and the porosity is below 20%.

DOWNHOLE MEASUREMENTS

Logging Operations and Quality of Logs

At Site 965, we acquired a full suite of log data by using the split Quad combination (DIT, SDT, HLDT, and CNT) and the Formation MicroScanner tool strings (see "Explanatory Notes" chapter, this volume). The NGT was attached to the top of each tool string and the Lamont-Doherty TLT was attached to the bottom of the Quad combo tool string for both runs. After coring and drilling operations were completed in Hole 965A, the borehole was conditioned with 9-ppg sepiolite/seawater drilling mud. The base of the BHA was set at 89.2 mbsf to start logging and pulled up to a position of 73.3 mbsf to maximize the logging interval. Table 12 summarizes the intervals logged with each tool string.

The quality of the log data ranges from fair to good. The sonic log recorded with the SDT is noisy and requires reprocessing. The caliper, recorded with the density tool, indicated that the hole conditions were good enough to run the FMS, although there were some borehole washout intervals (119.3–134.3 and 85.5–89 mbsf) where the hole diameter exceeded 15 in. (Fig. 26).

The FMS tool string was used for the first time in academic research in the Mediterranean and provided high-resolution resistivity images of the borehole wall as well as measurements of the three vector components of the local magnetic field (GPIT) and borehole inclination, deviation, and diameter in two orthogonal directions. Preliminary shipboard processing and analysis indicate that the FMS produced good-quality high-resolution data. All pads were in contact with the borehole wall except for the washed-out intervals.

Results and Preliminary Interpretation

Logging results were useful in delineating lithostratigraphic changes and in characterizing the sedimentary facies at this site (Fig. 27) where the geology between approximately 30 and 250 mbsf is not well known owing to poor core recovery. The combination of the Quad combo tool-string logs and the preliminary processed FMS images allows us to differentiate and characterize the sediments within a rather homogeneous sequence. The materials show a very low radioactivity, in the range of 10 to 20 GAPI, which is typical of the predominantly carbonate lithology. The analysis of the natural gamma spectral data indicates that the highest values of gamma radioactivity (always below 30 GAPI) are related to uranium-rich intervals, and in this carbonate-rich sequence the most feasible interpretation is that the uranium is present in organic-matter-rich intervals.

The logged section was subdivided into three log-stratigraphic units (log units) based on distinct features and trends in physical properties, as reflected in the logs. Nevertheless, the materials logged in Hole 965A seem to be rather homogeneous and do not reflect dramatic changes in composition or texture. The log units would thus correspond essentially to sedimentary or diagenetic facies changes, and a proper sedimentological interpretation will require integration of the core facies description together with a more detailed analysis of the logs post-cruise.

Log Unit 1 (73.3–102.8 mbsf)

The base of log Unit 1 is distinguishable on all the standard logs by a change in log values (Fig. 27) and a remarkable facies change recorded on the FMS images. Toward the base of log Unit 1, where the materials are more conductive as observed on the FMS images, radioactivity is fairly low (about 10 GAPI), which indicates a low content of radioactive minerals and suggests a "muddy" composition for the conductive levels. A lens-shaped, highly resistive feature was recognized at 91.8 mbsf on the FMS images.

Log Unit 2 (102.8–217.3 mbsf)

The gamma-ray and photoelectric factor logs display features that indicate slight changes in rock composition throughout this unit. At least six sequences can be recognized (Fig. 27). The interpretation of these sequences requires integration of the existing core data and more detailed log analysis. The log features suggest that the changes observed are probably related to changes in texture and/or sedimentary structures and do not correspond to any major compositional change. Sequence boundaries are mostly coincident with the more radioactive intervals, and this fact suggests the presence of organic-rich sediments at the sequence boundaries. The FMS data confirm the existence of different facies intervals, which have boundaries coincident with higher conductivity intervals. A striking feature recognized on the FMS logs is that the uppermost part of this unit (102.8–120.3 mbsf) is characterized by thinly layered (a few millimeters to 6 cm) alternations of low to higher resistivity levels that show up as a characteristic "zebra-skin" image. From 120.3 to 217.3 mbsf, alternating intervals of higher and lower resistivity, cross lamination, and some fractures are also recognizable on the FMS images. At 194.8 mbsf, the standard logs reflect an abrupt change in log values, which is not expressed on the FMS images.

Log Unit 3 (217.3–249.3 mbsf)

Alternating meter-scale intervals (1 to 5 m) reflect differences in rock composition and/or texture (primary or diagenetic) in log Unit

Table 11. Units based on petrophysical data and their correlation to lithology and stratigraphy at Site 965.

Unit	Depth (mbsf)	Density	Water content and porosity	Lithology	Stratigraphic age
A	0–30	Low, gradual increase	High, gradual decrease	Unconsolidated sediment, nannofossil ooze, and sapropels	Pleistocene–early Pliocene
B	30–33	Intermediate	Intermediate	Hard clays with calcareous clasts	latest Miocene?
C	33–250	High	Low	Shallow-water carbonate rocks	Miocene

Subunits of Unit A	Depth (mbsf)	GRAPE density	DSV velocity and shear strength	MST velocity	NGR	Stratigraphic age
A1	0–10	Moderate increase	Moderate increase	Moderate increase	Stability (to 8 mbsf)	late early Pleistocene–Holocene
A2	10–20	Moderate increase	Stability	Stability	Scattered readings	middle Pliocene–early Pleistocene
A3	20–30	Abrupt increase	Discontinuity, abrupt decrease to 24 mbsf, and sharp increase at 24–30 mbsf	Abrupt increase	Abrupt increase	early–late early Pliocene

Note: Subunits of Unit A based on high-resolution MST data.

Table 12. Hole 965A logged depth intervals for the three tool strings.

String	Run	Open-hole depth (mbsf)	Open-hole depth (mbrf)	In-pipe depth (mbsf)	In-pipe depth (mbrf)	Tools
Seismic-stratigraphic	Down	73.3–249.3	1591–1767	0–73.3	1517.7–1591	NGT/SDT/DIT/TLT
	Up 1	249.3–73.3	1767–1591	73.3–0	1591–1517.7	
	Up 2 (repeat section)	132.3–73.3	1650–1591	73.3–0	1591–1519.7	
Litho-porosity	Up 1 (repeat section)	252.7–176.4	1770–1694.1			NGT/HLDT/CNT/TLT
	Up 2	250.3–73.3	1768–1591	73.3–63.8	1591–1581.5	
FMS	Up 1	253–73.3	1770.7–1591	73.3–65.9	1591–1583.6	NGT/GPIT/FMS
	Up 2	253.3–73.3	1771–1591	73.3–66.7	1591–1584.4	

3. The FMS images allow the characterization of this unit as more resistive than log Unit 2; this feature is recognizable also on the induction logs and indicates a lower porosity. Cross lamination can be inferred from the FMS images. A remarkable feature of the FMS images is an alternation of thin (millimeters to a few centimeters) and thick (30 cm to 2 m) beds. These alternations recognized on the FMS images also have an expression on the standard Quad combo logs as striking fluctuations of the PEF log values. The high values of PEF within a carbonate sequence observed between 228.3 and 231.3 mbsf and also above and below this interval correspond to a "bright" (highly resistive) interval on the FMS images and suggest the presence of a mineral other than calcium carbonate cementing or diagenetically replacing the rock. The hole condition (caliper) was good, and thus the log values are reliable and can be used quantitatively. PEF values up to a maximum of 9.3 would suggest the presence of an iron-rich carbonate such as ankerite.

Despite the low recovery, the combination of log data and core data suggests that the logged sequence in Hole 965A is a relatively homogeneous carbonate. Nevertheless, the log response reveals changes in rock texture that can explain the low recovery.

According to the core data, the intervals recognized within logging Unit 2 (Fig. 27) would correspond to carbonate facies changes. A detailed analysis of the processed FMS together with the Quad combo logs will allow a better characterization of facies changes within Units 2 and 3. The FMS images give a clear indication of fracturing within log Unit 3.

Temperature Logging Tool

Temperature measurements with the Lamont-Doherty TLT were made in Hole 965A during run 1 (seismic-stratigraphic combination) and run 2 (litho-porosity combination). Owing to problems of calibration of the tool during run 2 (for which an old temperature tool was used), only values from the first run are presented here.

Figure 28 shows the fast- and the slow-thermistor temperatures. The bottom-hole temperature measured varies between 15.55° and 15.80°C, respectively, for the fast and the slow thermistors, owing to the borehole still reequilibrating during acquisition. Anomalies such as this in the temperature profile may result from temperature disturbances, circulation of borehole fluids during operations, or fluid flow coming from the formation into the borehole. The gradient calculated from the temperature values becomes negative below 150 mbsf (Fig. 28), which suggests fluid flow. The average thermal gradient is about 5 K/km. Further processing of the recorded temperature data, together with operational data, should give more accurate temperature profiles that will allow better links to the properties of the surrounding rocks.

SUMMARY AND CONCLUSIONS

Drilling at Site 965 was the first of a north-south transect of sites designed to test the tectonic hypothesis that the Eratosthenes Seamount is a continental fragment that is in the process of collision and underthrusting along the Cyprus active margin to the north. Specific objectives were (1) to determine if there is evidence of tectonically induced subsidence during the Pliocene-Quaternary, possibly related to collision; (2) to determine the lithology, age, and paleoenvironments of a prominent reflector beneath the Pliocene-Quaternary succession; and (3) to determine the timing, magnitude, and rate of any tectonic subsidence at this site.

Hole 965A is located on the fault-controlled upper northern slope of the seamount. The site was chosen where seismically transparent reflectors, characteristic of the Eratosthenes plateau area, are greatly reduced, owing to mass wasting and/or nondeposition. The present-day bathymetry is relevant to the interpretation of Pliocene-Quaternary sedimentation at Hole 965A. A pre-spud survey revealed the ideal site location on the crest of a small (approximately 5 km wide) north-south-trending ridge. This is surrounded by fault scarps that are affected by active normal faulting and mass-wasting processes.

Hole 965A was drilled to a maximum depth of 250.4 mbsf. After excellent recovery and core quality in the upper part of the section, APC coring was terminated by hard layers at about 30 mbsf. The following XCB cores had greatly reduced recovery of limestones. Three lithostratigraphic units were recognized at Site 965:

Unit I comprises 23 m of unconsolidated, extensively bioturbated nannofossil muds and nannofossil oozes, with sporadic sapropels. The bedding ranges from horizontal to subhorizontal and locally tilted. Microfaults range from moderately to steeply inclined, with measurable throws of up to 15 cm. The upper portion of Unit I is dated as Pleistocene, followed by a hiatus between the early and late Pliocene. A second hiatus, of an estimated 0.75-m.y. duration, extends from the late Pliocene to the middle Pleistocene. Sediments below 23–24 mbsf are only sparsely fossiliferous and are provisionally dated as no older than 6 Ma (late Miocene), based on calcareous nannofossils. Reworked benthic foraminifers were locally observed in the lower part of the succession. Preliminary paleomagnetic data (incompletely demagnetized) indicate a reversed polarity interval from 8 to 10 mbsf, directly above the first paleontologically determined hiatus, within the middle Matuyama Chron. Geochemical data from Unit I indicate that the chlorinity values are slightly less than that of seawater, as also noted in piston cores taken farther south on the Eratosthenes Seamount (i.e., at the KC20 site; G. de Lange, pers. comm., 1995). Organic carbon determinations range from 2% to 5% in sapropels, and the C/N ratios are suggestive of mixed marine and terrestrial origins for the organic matter.

Unit II comprises approximately 6 m of greenish and brownish sticky to firm clays, with scattered small (centimeter-sized), angular carbonate clasts. There is abundant evidence of soft-sediment deformation and reworking by gravity processes (e.g., as debris flows). Microscopy and XRD revealed significant occurrences of aragonite and dolomite, as well as locally abundant ostracode carapaces.

Unit III is a 200-m-thick interval in which the lithologies that were recovered range from medium- to coarse-grained, parallel- to cross-laminated packstones and grainstones (i.e., limestones), with common well-preserved calcareous algae (including oncolites and intact rhodoliths), ooids, echinoderm remains, pelecypods, benthic foraminifers, gastropods, and rare coral of poritid type. The oolitic lithofacies are mainly in the upper part of the section. The high porosity and permeability reflect the dissolution of aragonitic constituents. Interstitial and void-filling sparry calcite cement is sparse to well developed. Some limestones grade into poorly cemented gray marls, possibly indicative of the lithology of the nonrecovered intervals. The limestones are cut by sporadic carbonate veins, which suggest tectonic disruption. The final core showed evidence of penecontemporaneous tectonic brecciation and reworking of clasts.

An excellent suite of logs was obtained over 186 m. Interpretation of the FMS records, combined with other logs, reveals that (1) dips are nearly horizontal throughout; (2) the lower part of the succession includes apparent cross lamination, whereas the upper part is more planar bedded; (3) a mainly muddy succession is interbedded with thin intervals, interpreted as the cored limestones; and (4) scattered high-angle faults are present.

The preserved stratigraphic record at Site 695 began in the pre-early Pliocene (possibly late Miocene), with the accumulation of shallow-water carbonates in a muddy, current-influenced, probably lagoonal setting, adjacent to reef buildups and subject to tectonic instability. This was followed by the accumulation of calcareous clays in possibly low-salinity to hypersaline settings (Messinian?). Concomitantly with, or soon after, deposition, the muds were redeposited downslope into an open-marine setting (younger than 6 Ma). Subsequent Pliocene-Quaternary deep-marine sedimentation took place on a tectonically unstable slope, subject to slumping, nondeposition, and/or reworking.

In summary, at Site 965 on the Eratosthenes Seamount, a mainly shallow-water carbonate succession has subsided strongly during the last 5 Ma, accompanied by tectonic instability and faulting. Later faulting has produced the present fault-controlled bathymetry of the site. It is hoped that post-cruise studies will clarify the age of the shallow-water limestones and rate of tectonic subsidence. Drilling at Site 965 was clearly successful and constituted an important part of the test of the collision-related hypothesis for the evolution of the Eratosthenes Seamount.

REFERENCES

Alibes, B., Campo, M., Fraile, J., Galindo-Zaldivar, J., Fomenko, V., and Nieto, L., 1994. Sidescan sonar survey, OKEAN sonographs. *In* Limonov, A.F., Woodside, J.M., and Ivanov, M.K. (Eds.), *Mud Volcanism in the Mediterranean and Black Seas and Shallow Structure of the Eratosthenes Seamount.* UNESCO Rep. Mar. Sci., 64:128–134.

Beijdorff, K., van der Werff, W., and Gubanov, Yu., 1994. MAK-1 sonographs and profiles. *In* Limonov, A.F., Woodside, J.M. and Ivanov, M.K. (Eds.), *Mud Volcanism in the Mediterranean and Black Seas and Shallow Structure of the Eratosthenes Seamount.* UNESCO Rep. Mar. Sci., 64:129–133.

Channell, J.E.T., Di Stefano, E., and Sprovieri, R., 1992. Calcareous plankton biostratigraphy, magnetostratigraphy and paleoclimatic history of the Plio-Pleistocene Monte S. Nicola section (Southern Sicily). *Boll. Soc. Paleontol. Ital.,* 31:351–382.

Cita, M.B., 1975. Planktonic foraminiferal biozonation of the Mediterranean Pliocene deep-sea record: a revision. *Riv. Ital. Paleontol. Stratigr.,* 81:527–544.

Driever, B.W.M., 1981. A quantitative study of Pilocene associations of *Discoaster* from the Mediterranean. *Proc. K. Ned. Akad. Wet.,* 84:437–455.

Limonov, A., and Woodside, J., 1994. Results 4.2.1a. Seismic reflection profiling. *In* Limonov, A.F., Woodside, J.M., and Ivanov, M.K. (Eds.), *Mud Volcanism in the Mediterranean and Black Seas and Shallow Structure of the Eratosthenes Seamount.* UNESCO Rep. Mar. Sci., 64:120–127.

Limonov, A.F., Woodside, J.M., and Ivanov, M.K. (Eds.), 1994. *Mud Volcanism in the Mediterranean and Black Seas and Shallow Structure of the Eratosthenes Seamount.* Initial Results of the Geological and Geophysical Investigations during the Third "Training-through-Research" Cruise of the *R/V Gelendzhik* (June–July 1993). UNESCO Rep. Mar. Sci., 64.

Lucchi, R., Pott, M., Ivanova, E., Lottotskaya, A., Glover, C., Flecker, R., Basov, E., Kidd, R., and Robertson, A.H.F. 1994. Bottom sampling. *In* Limanov, A.F., Woodside, J.M., and Ivanov, M.K. (Eds.), *Mud Volcanism in the Mediterranean and Black Seas and Shallow Structure of the Eratosthenes Seamount.* UNESCO Rep. Mar. Sci., 64:134–135.

Rio, D., Raffi, I., and Villa, G., 1990. Pliocene-Pleistocene calcareous nannofossil distribution patterns in the Western Mediterranean. *In* Kastens, K.A., Mascle, J., et al., *Proc. ODP, Sci. Results,* 107: College Station, TX (Ocean Drilling Program), 513–533.

Robertson, A.H.F., 1990. Tectonic evolution of Cyprus. *In* Malpas, J., Moores, E.M., Panayiotou, A., and Xenophontos, C. (Eds.), *Ophiolites: Oceanic Crustal Analogues: Proc. Symp. "Troodos 1987":* Nicosia, Cyprus (Minist. Agric. Nat. Resour.), 235–250.

Robertson, A.H.F., Eaton, S., Follows, E.J., and McCallum, J.E., 1991. The role of local tectonics versus global sea-level change in the Neogene evolution of the Cyprus active margin. *Spec. Publ. Int. Assoc. Sediment.,* 12:331–369.

Robertson, A.H.F., Kidd, R.B., Ivanov, M.K. Limonov, A.F., Woodside, J.M., Galindo-Zaldivar, J., Nieto, L., and the Scientific Party of the 1993 TTR-3 Cruise, 1994a. Probing continental collision in the Mediterranean Sea. *Eos,* 75:233, 239.

Robertson, A.H.F., Kidd, R.B., Ivanov, M.K., Limonov, A.F., Woodside, J.M., Galindo-Zaldivar, J., Nieto, L., and the Scientific Party of the 1993 TTR-3 Cruise, 1995. Eratosthenes Seamount, easternmost Mediterranean: evidence of active collapse and underthrusting beneath the Cyprus active margin. *Terra Nova,* 7:254–264.

Robertson, A.H.F., Woodside, J.M., and Kidd, R., 1994b. Eratosthenes Seamount (study area 3). 4.1. Geological setting. *In* Limanov, A.F., Woodside, J.M., and Ivanov, M.K. (Eds.), *Mud Volcanism in the Mediterranean and Black Seas and Shallow Structure of the Eratosthenes Seamount.* UNESCO Rep. Mar. Sci., 64:115–119.

Spiegler, D., and Rögl, F., 1992. Bolboforma (Protophyta, incertae sedis) im Oligozän und Miozän des Mediterran und der Zentralen Paratethys. *Ann. Naturhist. Mus. Wien,* 94:59–95.

Sprovieri, R., 1993. Pliocene–early Pleistocene astronomically forced planktonic Foraminifera abundance fluctuations and chronology of Mediterranean calcareous plankton bio-events. *Riv. Ital. Paleontol. Stratigr.,* 99:371–414.

Ms 160IR-106

NOTE: Core-description forms ("barrel sheets") and core photographs can be found in Section 5, beginning on page 535. Forms containing smear-slide data can be found in Section 6, beginning on page 951. Color reflectance, physical properties, chemistry, and thin-section data are presented on the CD-ROM (back pocket).

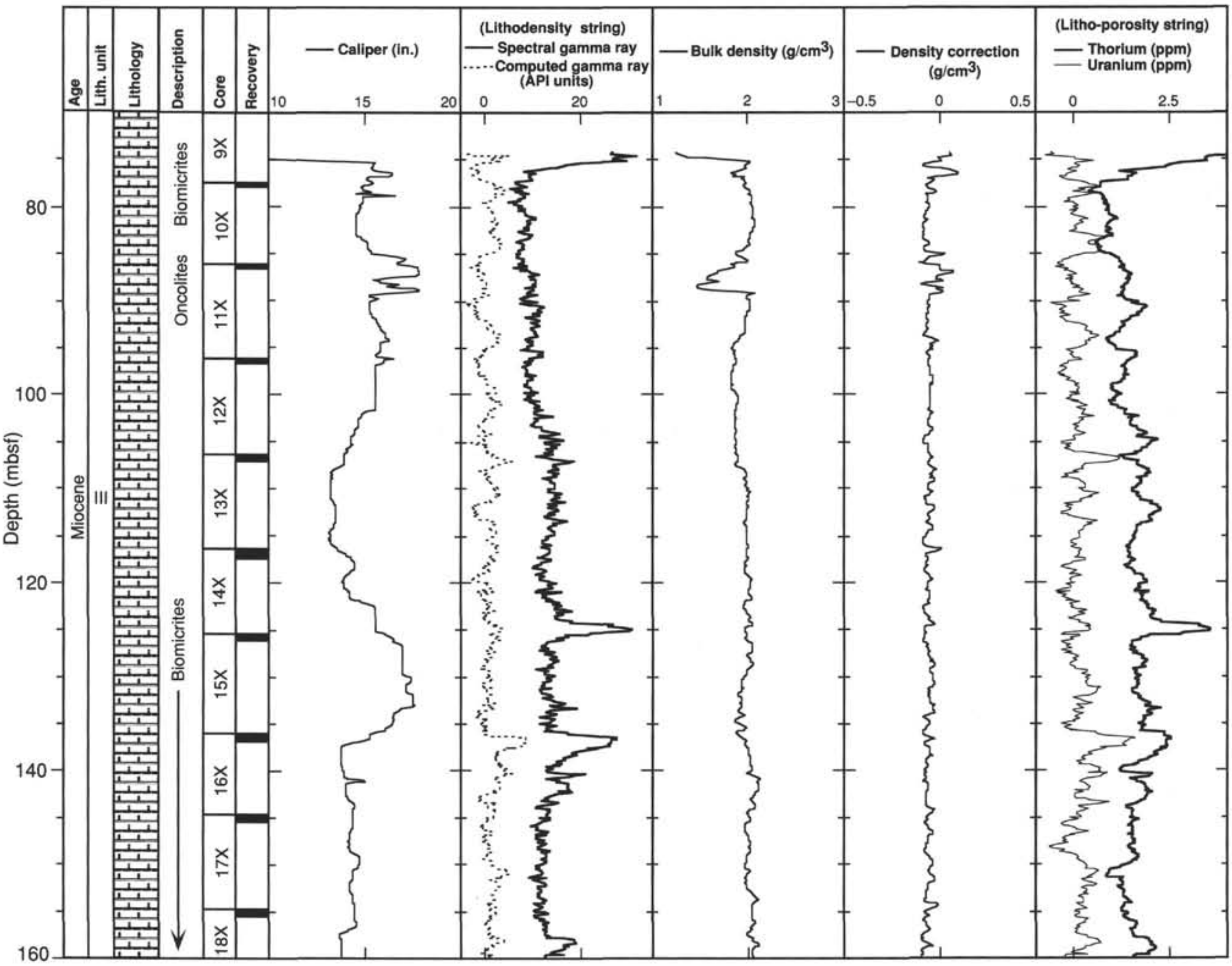

Figure 26. Hole 965A Quad combination tool and FMS (4-arm) caliper results.

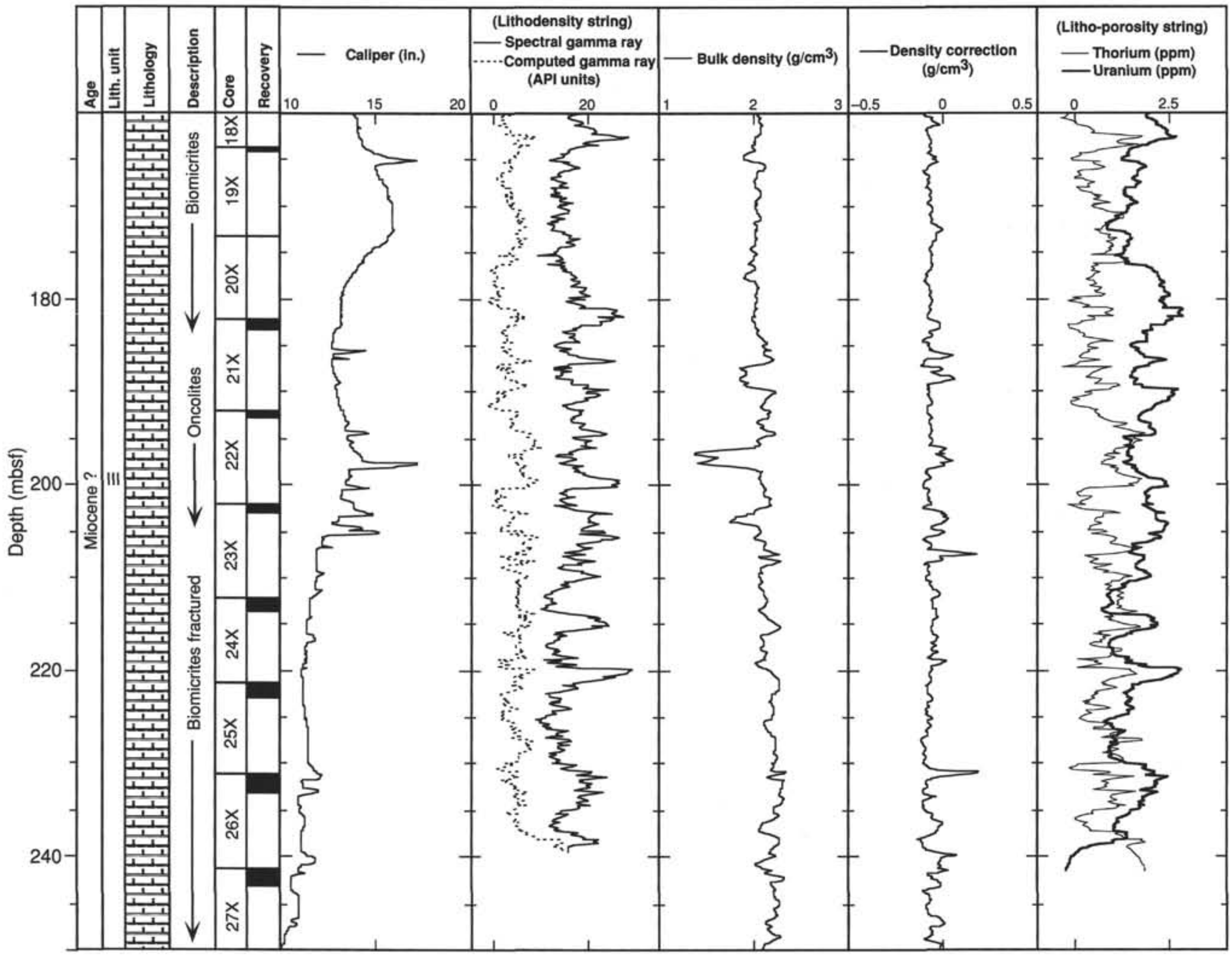

Figure 26 (continued).

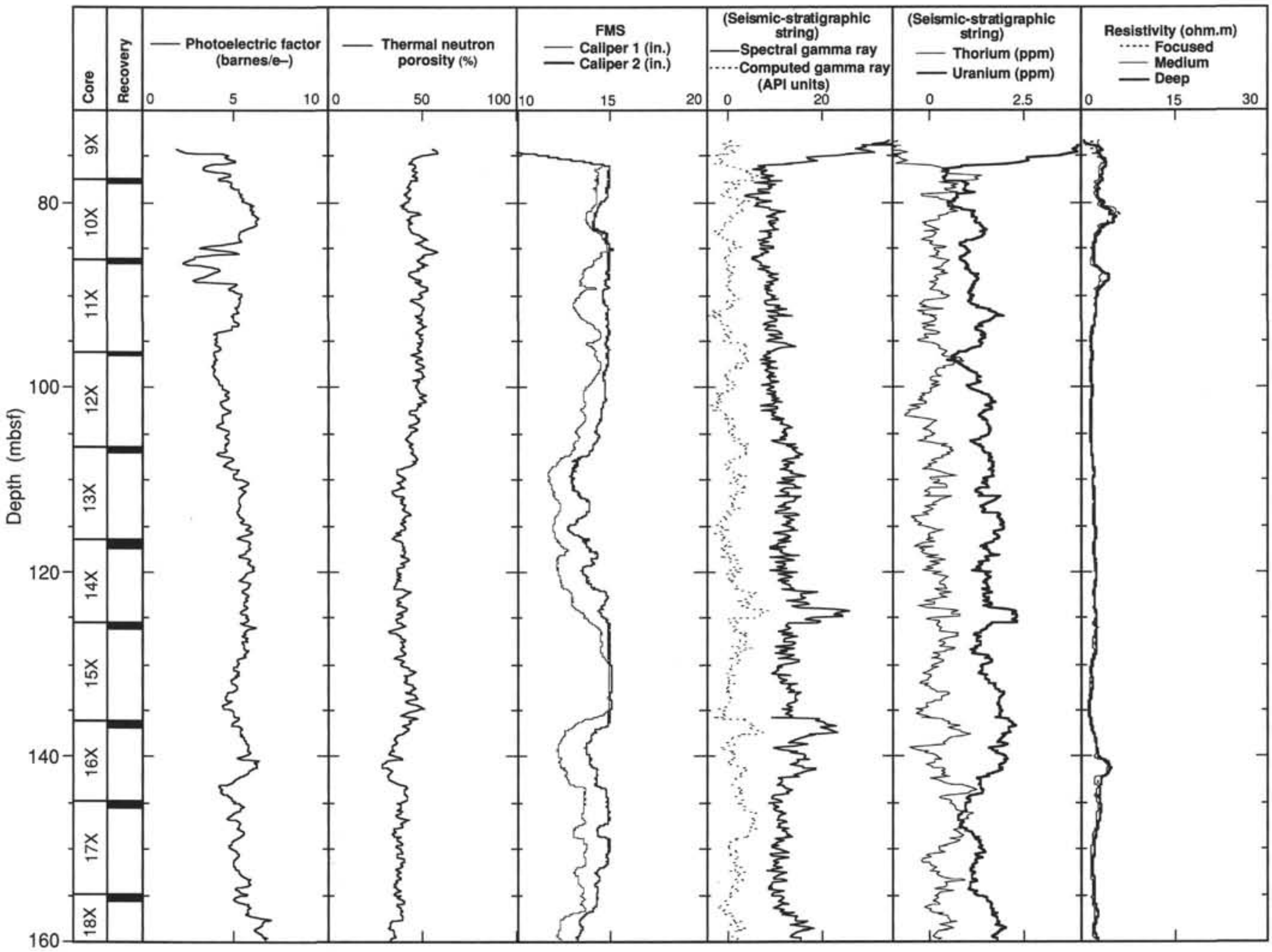

Figure 26 (continued).

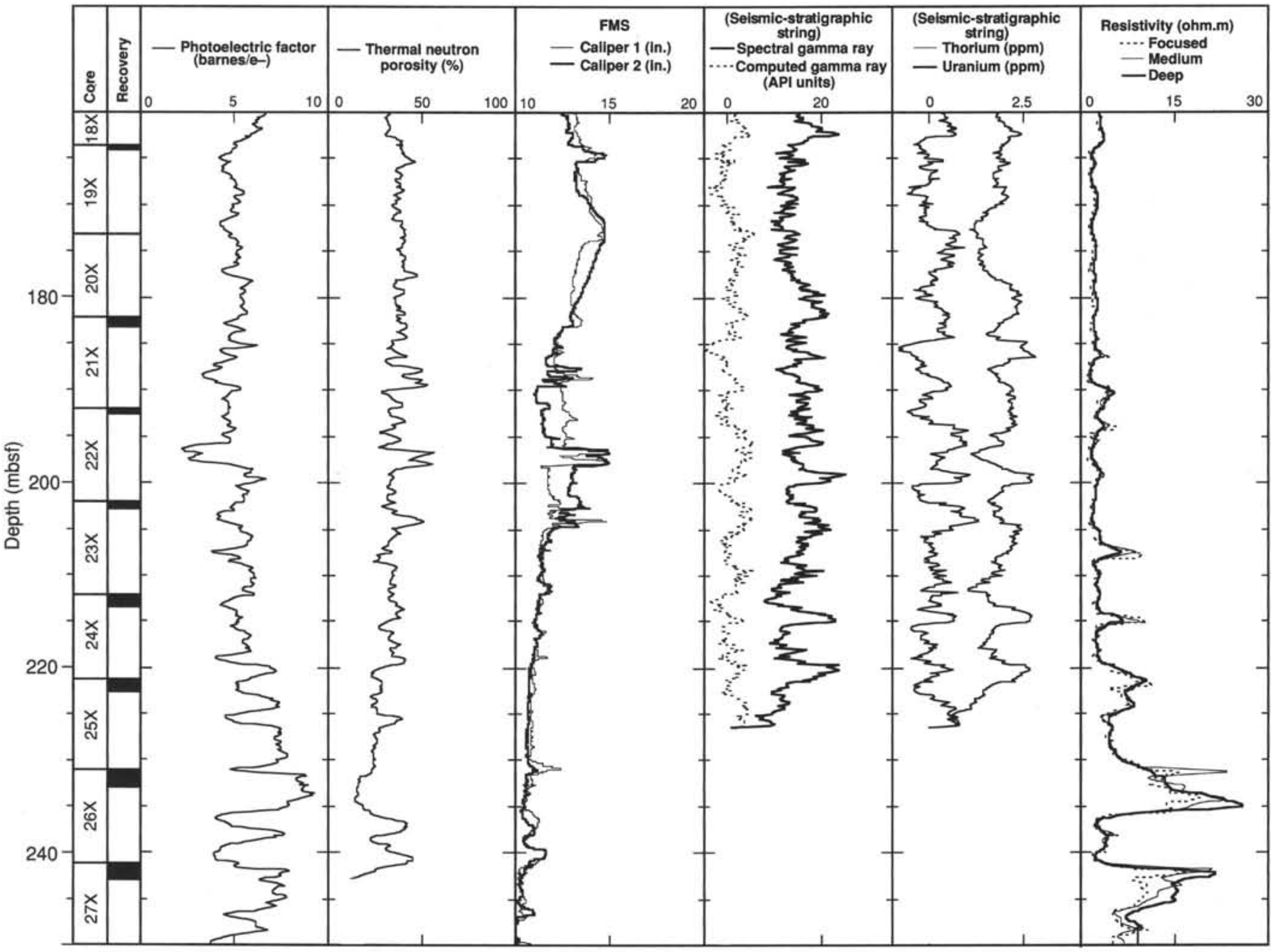

Figure 26 (continued).

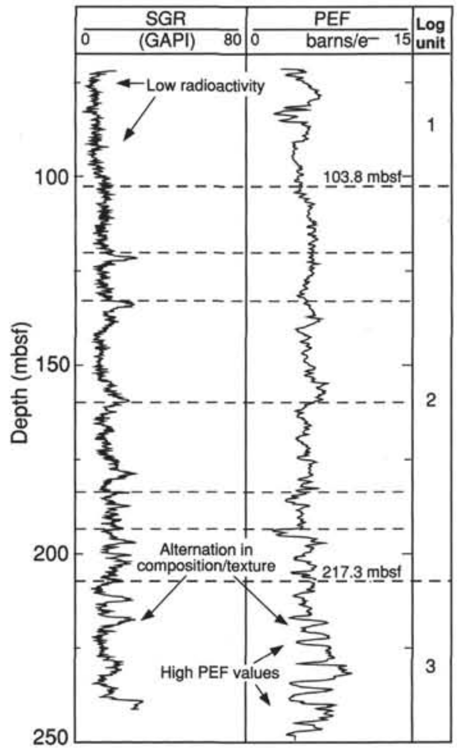

Figure 27. Interpreted log Units 1 through 3 in Hole 965A. The SGR and PEF logs show the most significant changes. The dotted lines within log Unit 2 indicate the occurrence of slight changes in log character that might correspond to boundaries between sedimentary sequences.

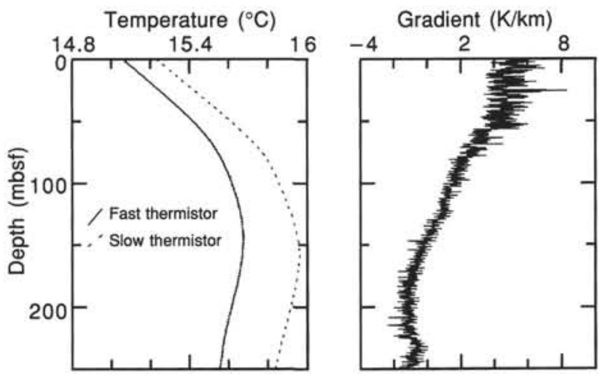

Figure 28. Data from the first run of the temperature logging tool in Hole 965A.

SHORE-BASED LOG PROCESSING
HOLE 965A

Bottom felt: 1517.7 mbrf
Total penetration: 250.4 mbsf
Total core recovered: 42.8 m (17.1%)

Logging Runs

Logging string 1: DIT/SDT-array/NGT
Logging string 2: HLDT/CNT/NGT
Logging string 3: FMS/GPIT/NGT (2 passes)

The wireline heave compensator was used to counter ship heave resulting from the mild sea conditions.

Bottom-hole Assembly

The following depths for the BHA are as they appear on the logs after differential depth shift (see **Depth shift** section) and depth shift to the seafloor. As such, there might be a discrepancy with the original depths given by the drillers on board. Possible reasons for depth discrepancies are ship heave, use of wireline heave compensator, and drill string and/or wireline stretch.

DIT/SDT-array/NGT: BHA at ~75 mbsf.
HLDT/CNT/NGT: BHA at ~75 mbsf.
FMS/GPIT/NGT: BHA ~75 mbsf.

Processing

Depth shift: All original logs were interactively depth shifted with reference to the NGT from the DIT/SDT-array/NGT run and to the seafloor (1517.7 mbrf).

Gamma-ray processing: The NGT data were processed to correct for borehole size and type of drilling fluid.

Acoustic data processing: The sonic logs were processed to eliminate some of the noise and cycle skipping experienced during recording.

Quality Control

Data recorded through the BHA, such as the CNT and NGT data above 74 mbsf, should be used only qualitatively because of the attenuation on the incoming signal. Invalid NGT values were recorded at 46–51 mbsf.

The hole diameter was recorded by the hydraulic caliper on the HLDT tool (CALI) and the caliper on the FMS string (C1 and C2).

Details of the standard shore-based processing procedures are found in the "Explanatory Notes" chapter (this volume). For further information about the logs, please contact:

Cristina Broglia
Phone: 914-365-8343
Fax: 914-365-3182
E-mail: chris@ldeo.columbia.edu

Elizabeth Pratson
Phone: 914-365-8313
Fax: 914-365-3182
E-mail: beth@ldeo.columbia.edu

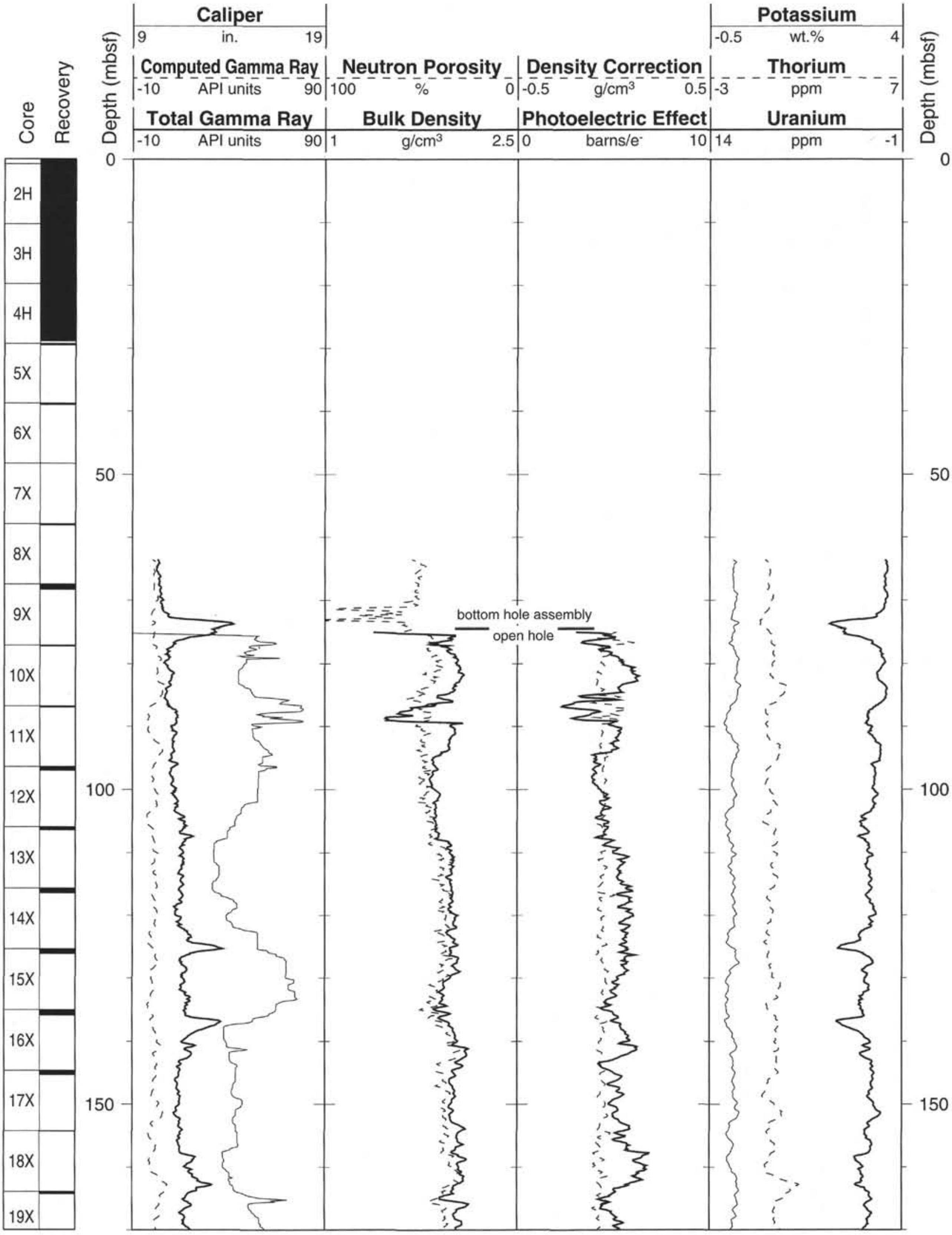
Core
Recovery
Depth (mbsf)
Caliper
9 in. 19
Computed Gamma Ray
-10 API units 90
Total Gamma Ray
-10 API units 90
Neutron Porosity
100 % 0
Bulk Density
1 g/cm3 2.5
Density Correction
-0.5 g/cm3 0.5
Photoelectric Effect
0 barns/e- 10
Potassium
-0.5 wt.% 4
Thorium
-3 ppm 7
Uranium
14 ppm -1
Depth (mbsf)
0
50
100
150
2H
3H
4H
5X
6X
7X
8X
9X
10X
11X
12X
13X
14X
15X
16X
17X
18X
19X
bottom hole assembly
open hole

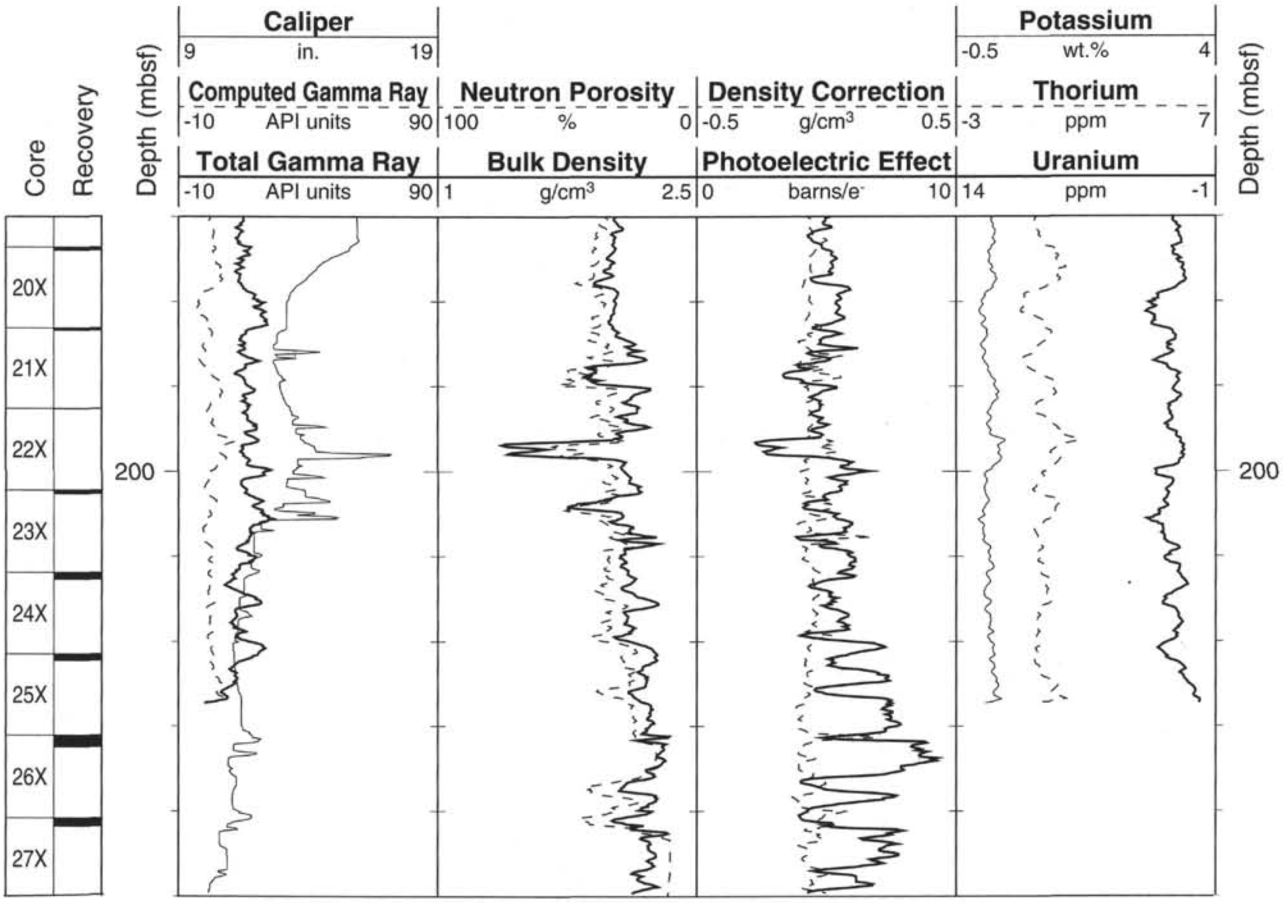

Core
Recovery
Depth (mbsf)
Caliper
9 in. 19
Computed Gamma Ray
-10 API units 90
Total Gamma Ray
-10 API units 90
Neutron Porosity
100 % 0
Bulk Density
1 g/cm3 2.5
Density Correction
-0.5 g/cm3 0.5
Photoelectric Effect
0 barns/e- 10
Potassium
-0.5 wt.% 4
Thorium
-3 ppm 7
Uranium
14 ppm -1
Depth (mbsf)
20X
21X
22X
23X
24X
25X
26X
27X
200
200

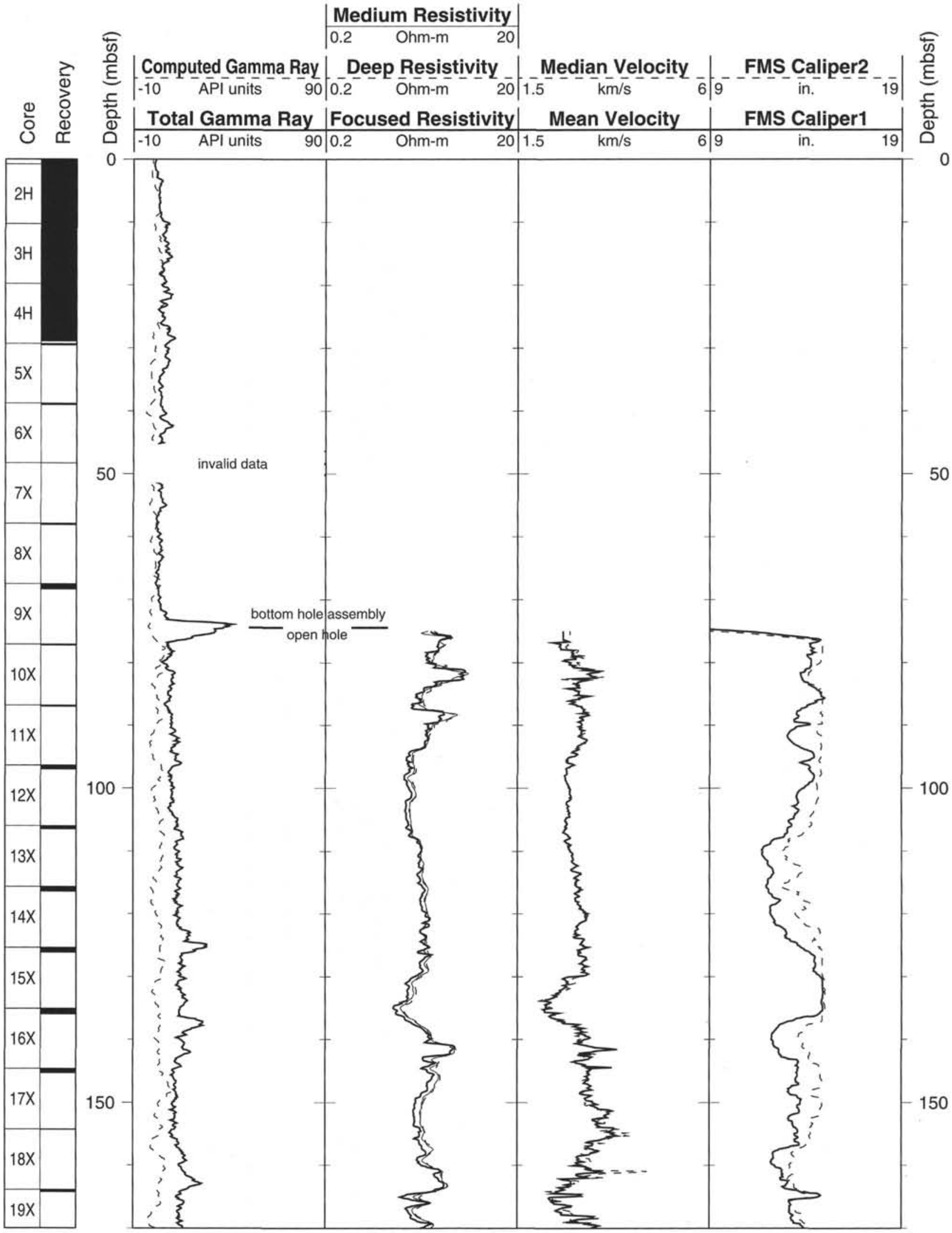
Medium Resistivity
0.2 Ohm-m 20
Computed Gamma Ray
-10 API units 90
Deep Resistivity
0.2 Ohm-m 20
Median Velocity
1.5 km/s 6
FMS Caliper2
9 in. 19
Total Gamma Ray
-10 API units 90
Focused Resistivity
0.2 Ohm-m 20
Mean Velocity
1.5 km/s 6
FMS Caliper1
9 in. 19
Core
Recovery
Depth (mbsf)
2H
3H
4H
5X
6X
7X
8X
9X
10X
11X
12X
13X
14X
15X
16X
17X
18X
19X
0
50
100
150
invalid data
bottom hole assembly
open hole

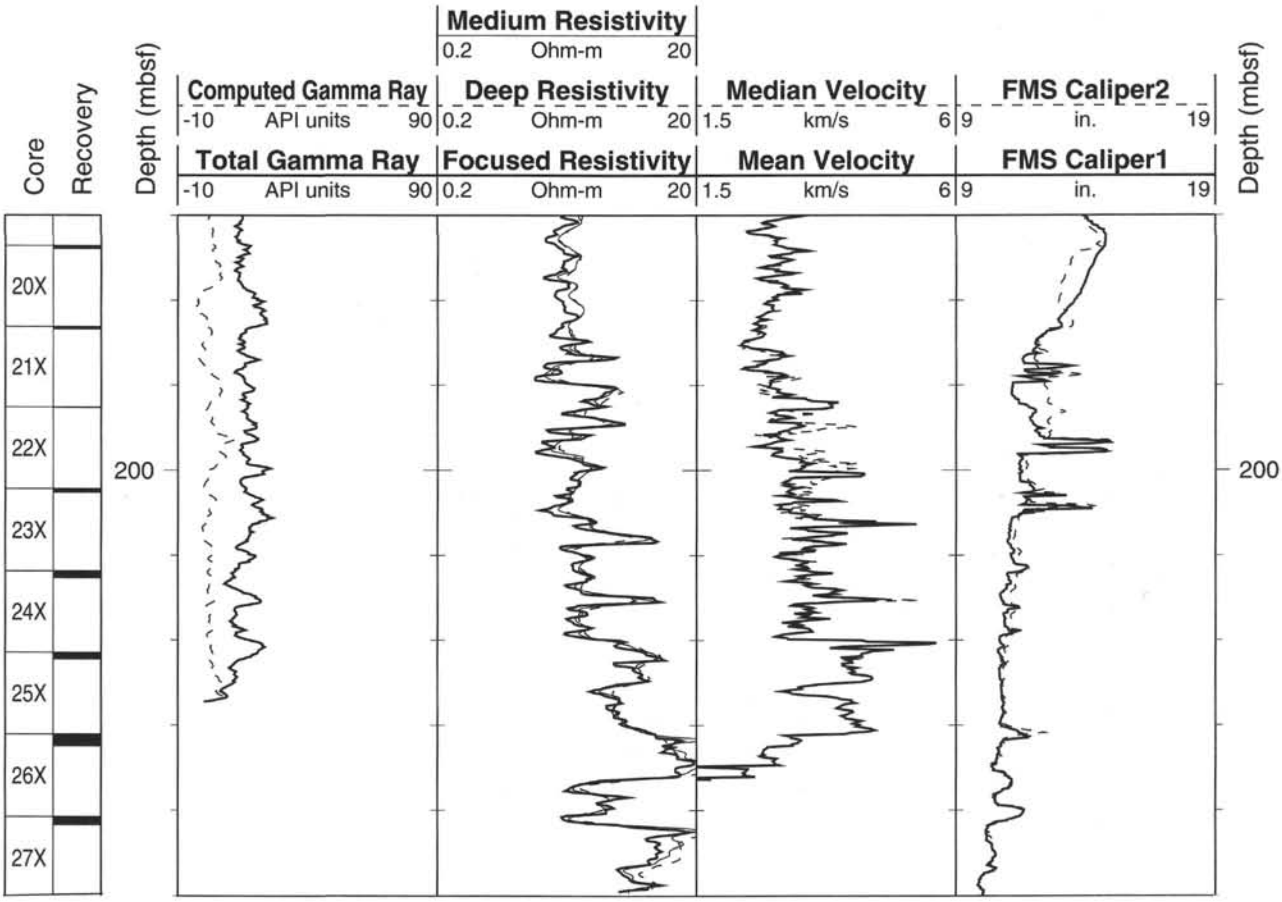
Core
Recovery
Depth (mbsf)
Computed Gamma Ray
-10 API units 90
Total Gamma Ray
-10 API units 90
Medium Resistivity
0.2 Ohm-m 20
Deep Resistivity
0.2 Ohm-m 20
Focused Resistivity
0.2 Ohm-m 20
Median Velocity
1.5 km/s 6
Mean Velocity
1.5 km/s 6
FMS Caliper2
9 in. 19
FMS Caliper1
9 in. 19
Depth (mbsf)
20X
21X
22X
23X
24X
25X
26X
27X
200
200